GEORGIA INSTITUTE OF TECHNOLOGY — OFFICE OF CONTRACT ADMINISTRATION

PROJECT ADMINISTRATION DATA SHEET

[x] ORIGINAL [ ] REVISION NO. _____

Project No. E-16-607 *

DATE 8/18/82

Project Director: Dr. S. G. Lekoudis

School/~~Lab~~ Aerospace Eng.

Sponsor: Lockheed-Georgia Company
Marietta, GA 30063

Type Agreement: P. O. No. CY67670

Award Period: From 7/1/82 To ~~12/31/82~~ (Performance) _____ (Reports)

Sponsor Amount: $15,000 (NTE) ~~1/31/83~~ Contracted through:

Cost Sharing: 12/31/83 GTRI/~~GIT~~

Title: Studies in Three-Dimensional Turbulent Boundary Layer Separation from Smooth Surfaces.

ADMINISTRATIVE DATA

OCA Contact Linda H. Bowman x4820

1) Sponsor Technical Contact:

Dr. H. Plumblee
Dept. 72-11, Zone 403
Lockheed-GA Company
Marietta, GA 30063

2) Sponsor Admin/Contractual Matters:

Mr. Bill Britton
Lockheed-Ga. Company
Mail Zone 630
Marietta, GA 30063

(404) 425-4535

Defense Priority Rating: NA

Security Classification: NA

RESTRICTIONS

See Attached NA Supplemental Information Sheet for Additional Requirements.

Travel: Foreign travel must have prior approval — Contact OCA in each case. Domestic travel requires sponsor approval where total will exceed greater of $500 or 125% of approved proposal budget category.

Equipment: Title vests with NA; none budgeted

COMMENTS:

* Continuation of E-16-606

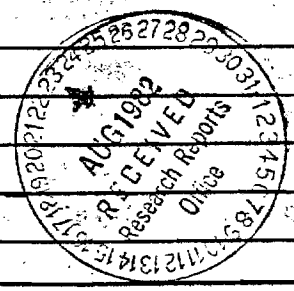

COPIES TO:

RAN

~~Administrative Coordinator~~
Research Property Management
Accounting
Procurement/EES Supply Services
~~Research Security Services~~
Reports Coordinator (OCA)
~~Legal Services (OCA)~~
Library
EES Public Relations (2)
~~Computer Input~~
Project File
Other GTRI

GEORGIA INSTITUTE OF TECHNOLOGY OFFICE OF CONTRACT ADMINISTRATION

SPONSORED PROJECT TERMINATION/CLOSEOUT SHEET

Date March 16, 1984

Project No. E-16-607 School/~~ESS~~ AE

Includes Subproject No.(s)

Project Director(s) Dr. S. G. Lekoudis GTRI / ~~XXX~~

Sponsor Lockheed – Georgia Co.

Title Studies in Three-Dimensional Turbulent Boundary Layer Separation from Smooth Surfaces

Effective Completion Date: 12/31/83 (Performance) 12/31/83 (Reports)

Grant/Contract Closeout Actions Remaining:

- [ ] None
- [x] Final Invoice or Final Fiscal Report
- [ ] Closing Documents
- [ ] Final Report of Inventions
- [ ] Govt. Property Inventory & Related Certificate
- [ ] Classified Material Certificate
- [ ] Other

Continues Project No. E-16-606 Continued by Project No.

COPIES TO:

Project Director
Research Administrative Network
Research Property Management
Accounting
Procurement/EES Supply Services
Research Security Services
Reports Coordinator (OCA)
Legal Services

Library
GTRI
Research Communications (2)
Project File
Other

Form OCA 60:1028

STUDIES IN THREE DIMENSIONAL TURBULENT BOUNDARY LAYER SEPARATION FROM SMOOTH SURFACES

Progress Report on Contract E-16-607
for the period June 1, 1981 through January 31, 1983

Prepared by

S. G. Lekoudis

Submitted to

The Advanced Research Organization of
the Lockheed-Georgia Company

SUMMARY

This report summarizes results of research done by the author, at Georgia Tech, with the support of the Advanced Research Organization of the Lockheed-Georgia Company, in the period between June 1, 1981 and January 31, 1983. Two problems have been addressed. The shock/boundary layer interaction in two-dimensional transonic flow, and the three-dimensional separation of incompressible turbulent boundary layers.

TABLE OF CONTENTS

1. THE SHOCK/BOUNDARY LAYER INTERACTION PROBLEM

Unless grid refinement close to a shock is done, shock capturing numerical solutions of the equations of fluid motion (full potential or Navier-Stokes) will produce a smeared shock. Grid refinement is not needed in routine calculations because it does not affect much the prediction of lift. Higher order methods do improve the "crispness" of the shock (Reference 1) but the shock is still smeared. Then two questions arise. First, is the effect of the shock/boundary layer interaction (SBLI) weakened because of the smeared shock? And second, are the boundary layer equations capable of describing the interaction? The answers are probably yes and no respectively in supersonic flow, but the subject is controversial in transonic flow because the shocks are weak. Therefore a study was undertaken to answer these questions.

The study employed a local solution for the two-dimensional SBLI region, based on the linearized Navier-Stokes equations, developed over a number of years by Inger and his coworkers (Reference 2), and a viscous/inviscid interaction scheme. The code for the viscous/inviscid interaction procedure (Reference 3) is generally acknowledged as the best available. The results of this study, given in detail in Appendix A, can be summarized as follows. For low angles of attack and for shocks away from the trailing edge, the boundary layer equations are giving reliable answers. Otherwise, the SBLI region must be properly modeled.

M. M. Khan of Lockheed-Georgia further developed the code and compared the predictions with measurements. The same general conclusions were found in these comparisons (Reference 4). From this work it is concluded that the proper treatment of the SBLI is necessary for the higher lift region of transonic airfoils (high angle of attack, shocks close to the trailing edge).

2. THE THREE-DIMENSIONAL SEPARATION PROBLEM

Three-dimensional Navier-Stokes solvers require considerable computer resources and their capability to resolve details in high Reynolds number flow is still a subject for research. Therefore viscid/inviscid interaction procedures are desirable both for attached or separated three-dimensional flows. In these procedures the question of what equations to use in the region close to separation arises.

In two dimensions, inverse boundary layer calculations have proven capable of accurately modeling certain flows with separation. Therefore the extension of these calculations to three-dimensional flows would offer the advantages of the boundary layer calculations. These are the low computer resource requirements and the high resolution capability. Such calculations have been done and compared with measured data. The details are given in the Appendix B. Similar calculations have been done by workers at O.N.E.R.A. (Reference 5). Thus, the capability of the technique to capture details inside the region of three-dimensional and separated flow at high Reynolds numbers is established.

3. PUBLICATIONS

The following publications are the result of the research described in Sections 1 and 2.

Non refereed publications

1. "Computation of viscous transonic flow around airfoils with trailing edge effects and proper treatment of the shock/boundary layer interaction region" by S. G. Lekoudis, G. R. Inger and M.M. Khan, AIAA Paper 82-0989

2. "Boundary layer calculations in the inverse mode for incompressible flows over infinite swept wings" by S. Radwan and S. G. Lekoudis, AIAA Paper 83-0454.

Refereed journal articles

The first of the two non-refereed publications has been accepted for publication in the Journal of Aircraft.

4. REFERENCES

L. "On various treatments of potential equations at shocks" by Chen L.T. and Caughey D.A. in NASA CP 2201, 1981.

2. "Some features of a shock-turbulent boundary layer interaction theory in transonic flowfields" by G. Inger in AGARD CP-291, 1981.

3. "Turbulent interactions on airfoils at transonic speeds - recent developments" by R. Melnik in AGARD CP-291, 1981.

4. "The aerodynamic effects of shock/boundary layer interactions on selected supercritical airfoils" by M. M. Khan and P. D. Dean, LG 82ER0173.

5. "A finite difference method for inverse solutions of 3-D turbulent boundary-layer flow" by Delery J. M. and Formery M.J., AIAA paper 83-0301.

APPENDIX A

AIAA-82-0989
Computation of the Viscous Transonic Flow Around Airfoils with Trailing Edge Effects and Proper Treatment of the Shock/Boundary Layer Interaction

S.G. Lekoudis, Georgia Institute of Technology, Atlanta, GA; and G.R. Inger, Univ. of Colorado, Boulder, CO; and M. Khan, Lockheed-Georgia Co., Atlanta, GA

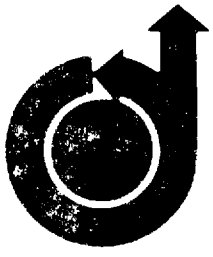

AIAA/ASME 3rd Joint Thermophysics, Fluids, Plasma and Heat Transfer Conference

June 7-11, 1982/St. Louis, Missouri

COMPUTATION OF THE VISCOUS TRANSONIC FLOW AROUND AIRFOILS WITH TRAILING EDGE EFFECTS AND PROPER TREATMENT OF THE SHOCK BOUNDARY LAYER INTERACTION

S. G. Lekoudis*
Georgia Institute of Technology
Atlanta, Georgia

G. R. Inger**
University of Colorado
Boulder, Colorado

M. M. S. Khan †
Lockheed-Georgia Company
Marietta, Georgia

Abstract

A viscous/inviscid interaction procedure is developed, for computing steady transonic flows over single airfoils. The procedure combines the method used in the GRUMFOIL code, developed by Melnik and his coworkers, with a basic solution for transonic shock/boundary layer interactions developed by Inger and his coworkers. Thus, the strong interactions occurring at the trailing edge and at the root of the shock are both taken into account. The procedure has been applied to non-separating flows on three airfoils.

For airfoil shock locations around mid-chord, it was found that marching under the shock using boundary layer theory gives similar results as the use of a detailed interaction theory except for significant overpredictions of displacement thickness rise and skin friction drop for 10-20% chord downstream. However, the two procedures give significantly different results when the shock position is rearward (70% chord or more); then the detailed interaction module alters the flow all the way to the trailing edge with consequent global effects on shock location and lift.

List of Symbols

C : airfoil chord

C_E : entrainment function $= \frac{1}{\rho_e u_e} \frac{d}{ds} (\rho_e u_e H_1 \theta)$

C_F : skin friction coefficient

C_p : pressure coefficient

C_L : lift coefficient

C_D : drag coefficient

C_M : moment coefficient

H_i : "incompressible" shape factor

H_1 : $\frac{\delta - \delta^*}{\theta}$

s : surface coordinate

SBLI : Shock/Boundary Layer Interaction

Greek Symbols

α : angle of attack

δ^* : displacement thickness

θ : momentum thickness

ρ : density

ν : kinematic viscosity

Subscripts

e : boundary layer edge conditions

∞ : freestream conditions

1. Introduction

The transonic flow around airfoils can be influenced to a large degree by viscous effects (Reference 1). Thus, detailed design of such airfoils requires the capability of accurately predicting the viscous effects. There are two ways of obtaining this capability, both being pursued vigorously. The first is to solve the two-dimensional Navier-Stokes equations for the whole flowfield. Although this is the most complete model, it needs significant computer resources because of the stringent requirements of adequate resolution of different parts of the flowfield. We will return to this point at another part of the discussion.

The second way of obtaining the predictive capability is through a composite approach involving viscous/inviscid interactions. This way solutions of different parts of the flowfield are combined in an iterative scheme. The scheme updates these solutions until convergence criteria are satisfied. Thus, the simplifying approximations, appropriate to the different parts of the flowfield, can be used to compute solutions efficiently. Reference 1 contains a number of different approaches and areas of application of viscous/inviscid interactions.

In general, the segmentation of the different areas of the flowfield is done according to the importance of viscosity. A classical segmentation is between inviscid parts of the flowfield, usually treated with a potential, and areas where the thin shear layer equations apply, the boundary layer and the wake. However this segmentation does not account for regions of the flowfield where both the streamwise pressure gradients and the role of

* Assistant Professor, School of Aerospace Engineering, Member AIAA.
** Professor and Chairman, Department of Aerospace Engineering Sciences. Associate Fellow. AIAA.
† Scientist Associate, Department 72/74. Member AIAA.

viscosity are important simultaneously. For the transonic flow around airfoils, such regions can be the shock/boundary layer interaction region and the trailing edge region. These regions are usually called the strong interaction regions.

The importance of these two regions has been examined before, but for each region individually. Melnik and his coworkers (Reference 2) have developed a code named GRUMFOIL, that computes the unseparated steady, transonic flowfield around airfoils using a lag-entrainment solution for the turbulent boundary layer. It also uses a special solution for the turbulent flow around the trailing edge, that accounts for the strong interactions that occur in that region. Boundary layer theory is used to march under the shock. The code has been validated at Lockheed-Georgia (Reference 3). It was found that the code produces satisfactory agreement with the experiments, for subcritical cases. It was also found that, sometimes, excessive Mach number corrections were needed to move the shock forward so that satisfactory agreement could be produced for supercritical cases. The effect of the tunnel walls in transonic flow does cloud the issue, when comparison with experiments is attempted. Because of this problem, no comparison with the experiments will be attempted in this paper. However, the importance of the findings of this work on the problem of comparing with experiments will be discussed.

Inger and his coworkers (References 4, 5) have developed a solution for the region of the interaction between a transonic normal shock and a turbulent boundary layer. The theory has been applied to the transonic flow around airfoils (Reference 6). It was shown that, depending on conditions such as the Reynolds number and the airfoil type, the influence of the shock in the subsequent development of the turbulent boundary layer can be significant.

The question that this work addresses is the following: What is the combined influence of the strong interactions, that occur at the trailing edge and the shock/boundary layer interaction region, in the prediction of the unseparated viscous, transonic flow around isolated airfoils? The tools used in answering this question are: the GRUMFOIL code and the shock/boundary layer interaction theory of Inger. The procedure used maintains the attractive features of viscous/inviscid coupling: good numerical resolution of the separately computed regions of the flow and fast execution on the computer. Briefly, the procedure works as follows. The GRUMFOIL code was modified so that the turbulent boundary layer calculations are discontinued in the shock region. The interaction theory of Inger is used to generate the boundary layer quantities after the shock region, where the boundary layer calculations are re-initiated. It is also used in the shock region to generate the entrainment velocities required for the viscous/inviscid coupling. Details of the procedure are given next.

2. The Viscous/Inviscid Interaction Procedure

The viscous/inviscid interaction procedure described in this paper, is based on incorporating a shock/boundary layer interaction module in the GRUMFOIL code. A schematic of the segmentation of the flowfield is given in Figure 1.

The inviscid part of the flow is computed using a conservative form of the full potential equation (Reference 2). Thus, isentropic flow was assumed across the shock. This is inappropriate for strong shocks, and for the airfoils examined, an error estimate is provided in GRUMFOIL. Consider the last supersonic point and, downstream of it, the first subsonic point in the shock region of the potential flow grid. The pressure coefficient, produced by the isentropic assumption, at the subsonic point, differs by less than 10% from the pressure coefficient generated using the Rankine-Hugoniot relationships. This happened at the airfoil "surface", the quotation marks indicating that the actual solution includes the displacement effects of viscosity. The total change in the pressure coefficient across the shock is greater than the difference between the pressure coefficients at the two mesh points mentioned, sometimes more than twice as large. Thus, although the preshock Mach number, in the cases examined, was never higher than 1.3, the possible error introduced by the isentropic approximation could be comparable with the changes due to the different treatment of the flow at the root of the shock. This error warrants further study using the Euler equations. No smoothing of the pressure distribution has been used in any of the calculations reported in this paper. Both first and second order differencing was tried for the supersonic regions. Practically no difference was found in the answers.

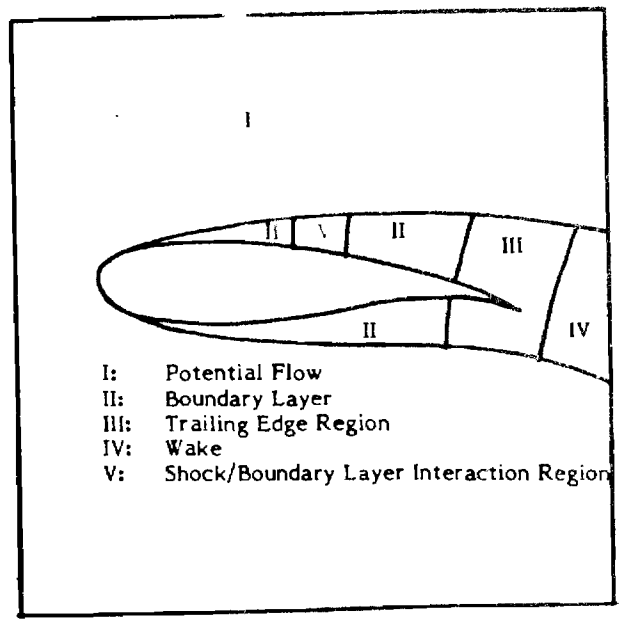

Figure 1. Schematic of the segmentation of the flowfield around a single airfoil.

The boundary layer solution in GRUMFOIL is based on a lag-entrainment method (Reference 7). A form of the kinetic energy equation for thin shear layers is used to generate an ordinary differential equation for the entrainment function C_E. The momentum integral equation and the conservation of mass are used to generate two more ordinary differential equations for the momentum thickness and the "incompressible" shape factor H_i. Thus, the boundary layer solution is based on an integral method. Neither the boundary layer theory, nor the approximations used in the kinetic energy equation are capable of handling very large adverse streamwise pressure gradients or non-negligible pressure gradients normal to the airfoil surface. At the airfoil trailing edge, when the flow is unseparated, a solution of the viscous equations based on asymptotic theory is used to cope with the problem. No such procedure existed in GRUMFOIL for treating the shock/boundary layer interaction region, and this study provides one. The reason for this study is not only the incorrect flowfield that might be computed by the boundary layer equations at the root of the shock, but the influence of the shock on the subsequent development of the boundary layer.

The method used to compute the shock/boundary layer interaction region for weak shocks was developed by Inger and his coworkers (Reference 4) using a non-asymptotic solution of the linearized Navier-Stokes equations. The solution has been expressed in a parametric form (Reference 5), the required input to the theory being the incoming boundary layer displacement thickness Reynolds number, the incompressible shape factor, and the pre-shock Mach number. Then the theory gives the pressure and skin friction distributions across the interaction zone, along with estimates of the extent of the interaction zone. The obliqueness of the shock is also taken into consideration (Reference 6).

In GRUMFOIL, the coupling between the inviscid part of the flow and the viscous parts is done by using the transpiration velocity. This velocity is computed from flow variables generated by the lag-entrainment method. Thus, in order to insert a local solution for the shock/boundary layer interaction region, the solution must be used to compute the transpiration velocity in the interaction region. This was done in the present study. However, before the insertion is accomplished, the location and the extend of the interaction region has to be determined.

2.1 Computing the Region of the Shock Boundary Layer Interaction

Because the boundary layer theory is not used under the shock, the ends of the interaction region have to be determined. The potential flow calculation and the viscous/inviscid coupling produce a smeared shock. Thus, the ends of the interaction region can be defined in a nonunique manner. There are two guides for their definition. The first is that the boundary layer calculations should not be subjected to the pressure rise at the shock. The second is the extent of the interaction region given from the interaction theory, for the particular combination of the incoming boundary layer properties and the preshock Mach number. It turns out that, unless the Reynolds number based on the airfoil chord and the freestream velocity is well below a million, the computed interaction length is shorter than the smeared shock width at the airfoil "surface". Thus, the need that the boundary layer will not be subjected to the pressure rise at the shock is used to determine the ends of the interaction zone.

A comment is appropriate at this point about numerical solutions of the Navier-Stokes equations because the interaction lengths, computed by Inger's theory, have been successfully compared with experiments (Reference 5). It would be appropriate that these lengths are considered in the numerical scheme and that enough grid points are used in the streamwise direction so that the interaction is properly computed. This seems necessary if flow quantities in that region need to be accurately predicted. However if that need does not exist, then the requirements for a dense grid exist only if the flow away from the shock/boundary layer interaction region is affected by the details of the flow at the interaction. The streamwise interaction lengths at high Reynolds numbers, above 10 million, can be shorter than 2% of the airfoil chord.

A schematic of the distribution of the pressure coefficient in the shock region is shown in Figure 2. The mesh points A and B satisfy the above-discussed requirements about the ends of the interaction zone. Considerable experimentation was done to determine a reliable way of finding the points A and B. These points vary in location during the iterative viscous/inviscid coupling. The point O is named the root of the shock in

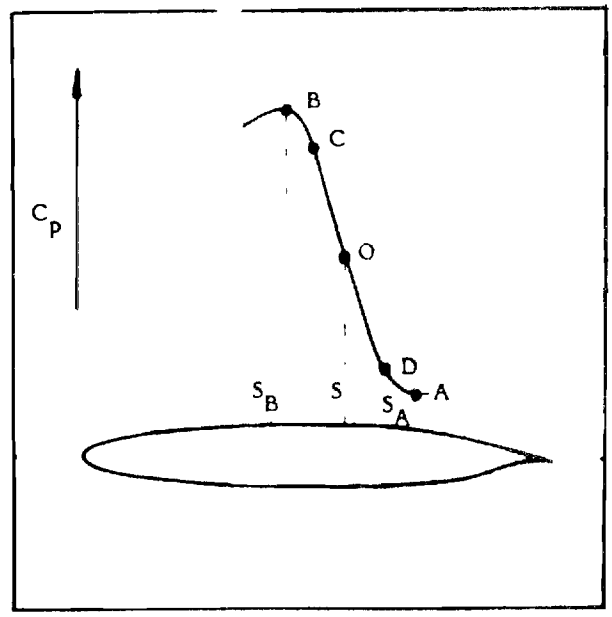

Figure 2. Schematic of Location of the Shock/Boundary Layer Interaction Region.

the potential flow grid. It was found that the results are not very sensitive to the location of O as long as O is between A and B. Thus, the following procedure was used to locate the interaction region.

The point O was defined as the last supersonic point in the potential flow calculation. The points A and B next to the neighboring points C and D, downstream and upstream of the point O respectively, were taken as the ends of the interaction region. However if the ratio

$$\frac{(C_p)_A - (C_p)_D}{(C_p)_D - (C_p)_O} \qquad (1)$$

and/or the ratio

$$\frac{(C_p)_B - (C_p)_C}{(C_p)_C - (C_p)_O} \qquad (2)$$

was less than a prescribed quantity, the point D and/or the point C marked the ends of the interaction region. Numerical experiments showed that .1 was a good value for the prescribed ratio and produced reliably the interaction region. Thus the interaction region extended at minimum between three, and at maximum between five points in the potential flow grid.

The interaction theory gives a continuous variation of the boundary layer parameters in the interaction region. A schematic of this variation is shown in Figure 3. The calculation of the potential flow requires these parameters only at discrete points. Because of the discussed mismatch between the streamwise interaction lengths provided by the theory, and the lengths resulting from the smearing of the shock, one must deal with a non-uniqueness in the treatment of the points C and D of Figure 9, when the smearing of the shock extends the interaction region between the points A and B. There are two alternatives. The first is to keep the boundary layer quantities "frozen" and equal to the end values. The second alternative is to use interpolated values between the values at the root of the shock, point O, and the

values at the ends of the interaction region, points A and B. Both options were used: it was found that the results were practically insensitive to the choice. Table 1 gives a comparison of the lift, drag, and moment coefficients for the RAE2822 airfoil, produced by the two alternatives discussed.

A test was performed to study the sensitivity of the results to the form of the interpolation. Both linear and exponential variation was assumed for the boundary layer properties in the interaction region. The last because, according to the interaction theory (Figure 3), the streamwise variation of the properties is negligible at the ends of the interaction region. The change in integral parameters like C_L, C_D, C_M and the shock location was affected by about 1% from the change in the type of the interpolation.

Another test was performed in order to study the sensitivity of the results to the extent of the interaction region. The boundary layer properties were kept "frozen", and equal to the values at point A, at the next location downstream of point A. It was found again that the resulting integral parameters like C_L, C_D, C_M and the shock location were practically insensitive to that change. Thus, all the values of the boundary layer properties at C and D were linearly interpolated from the values at O and A and B, and this applies to all the results shown in this paper.

2.2 The Viscous/Inviscid Coupling

A grid sequencing is used in the potential flow calculation in GRUMFOIL. The number of points used in the "wraparound" direction is 40, 80 and 160 as the grid becomes denser. In order to save time, the shock/boundary layer interaction is computed only in the dense grid. In the two coarse grids, boundary layer theory is used to march under the shock. There was no increase in the number of relaxation cycles necessary to converge, nor was there a need to change the relaxation parameters. As a result, there is practically no change in the run time of GRUMFOIL.

A parameter that affects the solution significantly in the shock region is the entrainment function C_E; relationships based on its definition are given in the Appendix. In the lag-entrainment system C_E is a dependent variable, related empirically with the kinetic energy of turbulence. The distinction between "equilibrium" and "non-equilibrium" values of C_E is used in formulating the lag-entrainment system. In the interaction calculations presented in this paper, C_E is explicitly computed from the boundary layer parameters given by the interaction theory. Because only the basic definition of C_E is used (see Appendix), there is no need to distinguish between its equilibrium and non-equilibrium values. It was found that, in general, the interaction theory gives lower values for C_E in the region after the shock than the lag-entrainment method.

3. Results

The developed viscous/inviscid coupling technique was applied to three airfoils. All of them are of the supercritical type. The reasons for choosing these airfoils follow.

The RAE 2822 airfoil has been used by Melnik and his coworkers to describe the capabilities of GRUMFOIL. Moreover it was used in Reference 3 to validate the code. Thus, there was previous experience in computing with this airfoil. The LG5-621, described in Reference 8, was

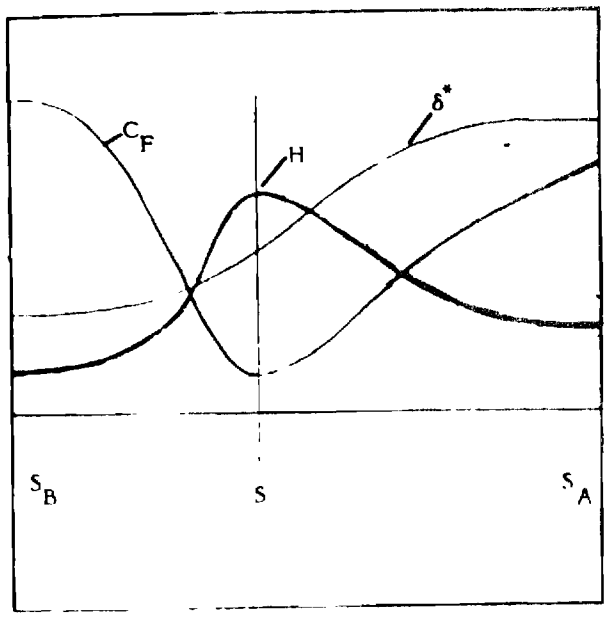

Figure 3. Schematic Variation of Boundary Layer Quantities in the Shock/Boundary Layer Interaction Region.

Table 1

RAE 2822, M = 0.73, R_C = 6 million

	Properties of C and D Same as B and A	Properties of C and D Interpolated
	$\alpha = 1.8^\circ$	
C_L	0.6267	0.6175
C_D	0.0099	0.0098
C_M	-0.0894	-0.0880
	$\alpha = 2.0^\circ$	
C_L	0.6643	0.6647
C_D	0.0107	0.0107
C_M	-0.0898	-0.0893
	$\alpha = 2.2^\circ$	
C_L	0.7302	0.7129
C_D	0.0118	0.0115
C_M	-0.0937	-0.0908
	$\alpha = 2.4^\circ$	
C_L	0.7573	0.7732
C_D	0.0132	0.0135
C_M	-0.0925	-0.0950

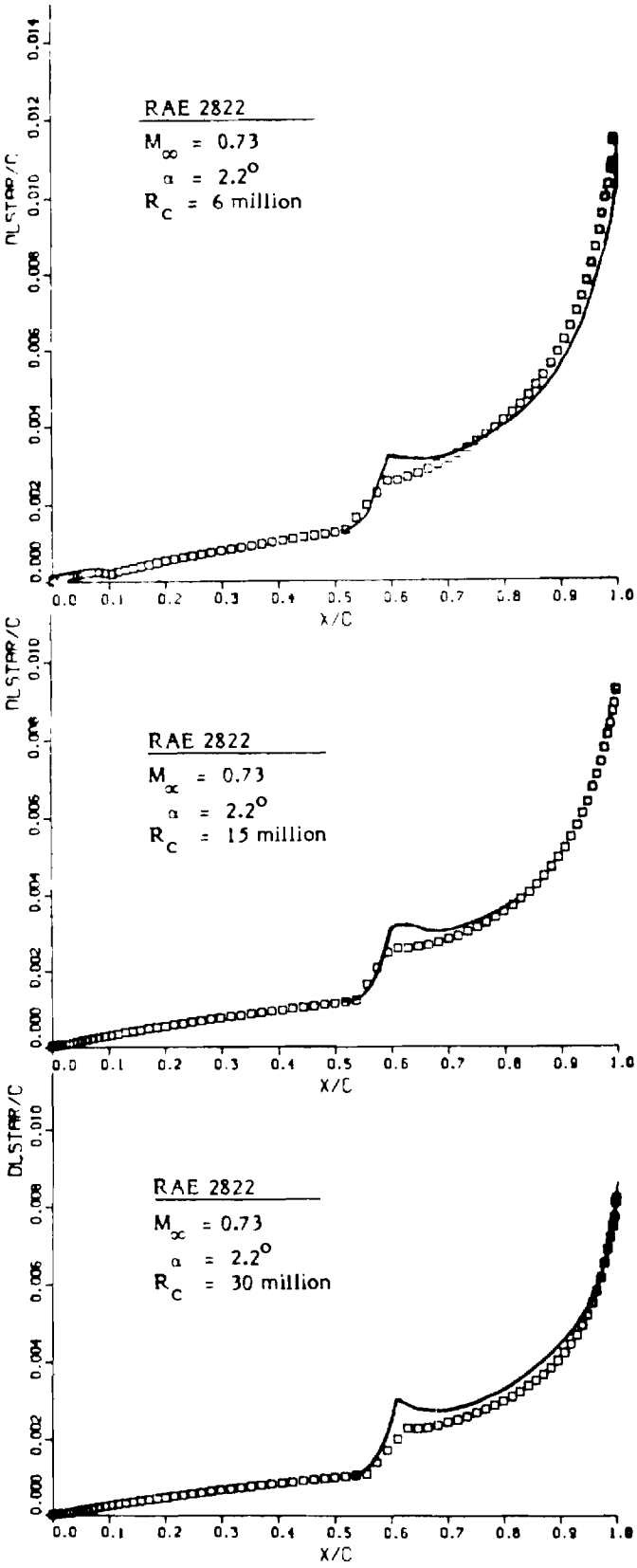

Figure 4. Variation of the displacement thickness with the SBLI theory (——) and without it (——)

chosen because it is a thick (21%) supercritical airfoil with a long region of adverse pressure gradient and, thus, a relatively thick boundary layer at the trailing edge. The third example, LG4-612, is a 12% thick supercritical airfoil and is described in Reference 9. The reason for choosing this airfoil is that an ongoing experimental program at Lockheed-Georgia aims at measuring flow quantities at the shock/boundary layer interaction region. GRUMFOIL itself was checked out by reproducing computed results provided by the Theoretical Aerodynamics Branch of the Langley Research Center.

A fairly large number of calculations was produced for the RAE 2822 airfoil, by varying the freestream Mach number, angle of attack and chord Reynolds number. However, only a small representative set of results will be presented here. Figures 4 through 9 show the computed displacement thicknesses and skin friction coefficients for the upper surface of the airfoil. They also show the resulting pressure coefficient distributions. These results are for two angles of attack, α = 2.2° and 2.4°, at M_∞ = 0.73. Note that for these angles of attack at the slightly higher Mach number M_∞ = 0.74, the shock induces separation at α = 2.4° and incipient separation close to α = 2.2°, as predicted by both the shock/boundary layer interaction theory (SBLI) and the lag-entrainment equations marched under the shock. For these moderately aft-loaded airfoil conditions with a relatively forward shock position around mid-chord (.50 < x/C < .60) the two ways of computing the shock/boundary layer interaction produce almost identical results for the pressure distribution and shock location. However, the detailed interaction effect on δ^* and C_f are seen to be more important at the larger angle of attack: improper modeling of the interaction overpredicts the δ^* increase and C_f drop up to 15-20% chord downstream.

Results for the somewhat lower Mach number operating conditions of the LG5-621 airfoil, where the shock is in fact forward of mid-chord (.40 < x/C < .50), are shown in Figs. 10-15 and yield similar conclusions. There are no noticeable interaction detail effects on the pressure distribution, while significant influence on the δ^* and C_f distributions can be seen 10-15% chord downstream at the higher angle of attack. It should be noted that for the two airfoils mentioned, further increases in the M_∞ lead to boundary layer separation using both the lag-entrainment equations and the SBLI theory; thus it was not possible to compute with shock closer to the trailing edge.

The operating conditions investigated for the third airfoil design LG4-612, unlike the other two, involve higher Mach numbers and hence much further aft shock locations (.60 < x/C < .80) without boundary layer separation occurring. In these cases, significant global as well as local influence of proper SBLI modeling is now observed as illustrated in Figs. 16-22. Typical results for M_∞ = 0.70 are shown in Figure 16. There is practically no difference in the results produced by the SBLI theory and the lag-entrainment method in this case, similar to the results found for the RAE and the LG5 airfoils. However, the situation changes rapidly as the Mach number increases and the shock moves aft. Thus, for the case of M_∞ = 0.735, Figures 17, 18 and 19 show displacement thicknesses, skin friction coefficients and pressure distributions, respectively, which differ noticeably when the SBLI theory is used instead of the boundary layer equations. Notice also that the shock location moves forward for α = 1.5° and backward for α = 2.1°; higher angles of attack indicate separation and invalidate the assumptions used in the calculations. For the case of M_∞ = 0.760, Figures 20, 21 and 22 show that the two procedures compute flow properties that vary quite

significantly. Indeed the shock is placed further downstream by the SBLI theory, and the influence of the interaction solution details now extends all the way to the trailing edge. These results confirm the original suggestions of Inger and Cantrell (See Ref. 5) and are also concordant with the findings of the interactive study by Nandanan et al.[6]

It should be mentioned that the differences in lift coefficients associated with the interactive-detail effects predicted for the LG5-621 cases shown in Figures 17-22 indicate changes comparable to the ones that could be obtained by applying Mach number corrections due to blockage in transonic wind tunnels. Thus for the cases shown, the proper treatment of the SBLI can be as important as these corrections and should be taken into consideration. Table 2 shows a comparison of lift, drag and moment coefficients obtained with and without using the interactive module for the conditions corresponding to Figures 20-22.

4. Concluding Remarks

A fundamentally-based shock/boundary layer interaction module has been incorporated into the state of the art viscous/inviscid coupling procedure. GRUMFOIL which computes the steady, unseparated transonic flow around single airfoils including the trailing edge interaction region.

For non-separating airfoil operating conditions involving shock locations around mid-chord, it was found that the boundary layer theory produces results that are comparable to those with the interaction module except for noticeable local overpredictions of displacement thickness rise and skin friction drop over distances of 15-20% chords downstream at the higher angles of attack. The results become more comparable as the Reynolds number increases. However, for airfoils that operate without separation at higher Mach numbers with more rearward (70% chord or more) shock locations, the results produced by the two methods are not only significantly different locally but also show noticeable global differences in shock location and lift. The results are in general agreement with the implications of several earlier studies[3,8]; moreover the conclusions are valid even as the flow approaches incipient separation.

From this investigation, it was found that the fact that GRUMFOIL sometimes produces shocks located after their measured positions is not due to the SBLI. However, for shocks well downstream of mid-chord ($x/C > .60$, say), it was found that the details of the SBLI can affect the downstream development of the boundary layer significantly and thus should be properly modeled in a viscous/inviscid coupling procedure.

Appendix

The entrainment function C_E is defined as

$$C_E = \frac{1}{\rho_e u_e} \frac{d}{dx} \int_o^\delta \rho u \, dy \qquad (A.1)$$

From the integrated continuity equation across the boundary layer, the streamline slope at the boundary layer edge is formally linked to this function by the general relationship

$$\frac{V_e}{U_e} = - C_E + \frac{d\delta}{dx} \qquad (A.2)$$

The strong influence of C_E on the inviscid "transpiration velocity" of the GRUMFOIL code is evident in Eqs. (A.2).

Instead of supplying an empirical formula for C_E, we may instead develop a basic relationship that links it directly to the local interaction properties, working directly from the RHS of Eq. A.1. Introducing the definition of δ^* and the shape factor $H = \delta^*/\theta$, we have upon neglecting $\partial p/\partial y$ across the boundary layer

$$C_E = \frac{d(\delta - \delta^*)}{dx} + (\delta - \delta^*) \frac{d \ln(\rho_e U_e)}{dx} \cong$$

$$\frac{d}{dx}\left(\frac{\delta}{\delta^*} - 1\right)H\theta + \left(\frac{\delta}{\delta^*} - 1\right)H\theta \left(\frac{M_e^2 - 1}{\gamma p_e M_e^2}\right) \frac{dp_e}{dx} \qquad (A.3)$$

Now for steady 2-D flow we can further introduce the compressible boundary layer momentum integral equation

$$\frac{d\theta}{dx} = \frac{C_f}{2} + \frac{dp_e/dx}{\gamma p_e M_e^2}(2 + H - M_e^2)\theta \qquad (A.4)$$

and thus express (A.3) as

$$C_E = H\left(\frac{\delta}{\delta^*} - 1\right)\left[\frac{C_f}{2} + \frac{(H+1)\theta dp_e/dx}{\gamma p_e M_e^2}\right] + \theta \frac{d}{dx}\left[H\left(\frac{\delta}{\delta^*} - 1\right)\right] \qquad (A.5)$$

This relationship can be used to find C_E along the interaction without empiricisms by means of the correct local interactive values inserted into the RHS, in particular, downstream of the interaction when the interactive pressure and integral parameter changes have died out (so that the last two terms of A.5 become negligible compared with the first), Eq. (A.5) simplifies the correct "reinitialized" positive value

$$C_{E_2} \approx H_2\left(\frac{\delta_2}{\delta^*_2} - 1\right)\frac{C_{f_2}}{2} \qquad (A.6)$$

for restarting the lag-entrainment turbulent boundary layer program. Equation (A.5) was in fact used in the present work for this purpose.

Table 2

LG4-612, $M = 0.76$, $R_c = 11$ million

	Without SBLI	With SBLI
	$\alpha = 1.1^o$	
C_L	.7349	.7695
C_D	.0157	.0167
C_M	-.1535	-.1625
	$\alpha = 1.2^o$	
C_L	.7527	.8252
C_D	.0166	.0192
C_M	-.1541	-.1746

Acknowledgements

The work was supported by Lockheed-Georgia's IR&D program. The first author was supported by a Grant from the Advanced Research Organization. The help of Harry Mead in understanding some of the internal structure of GRUMFOIL is appreciated.

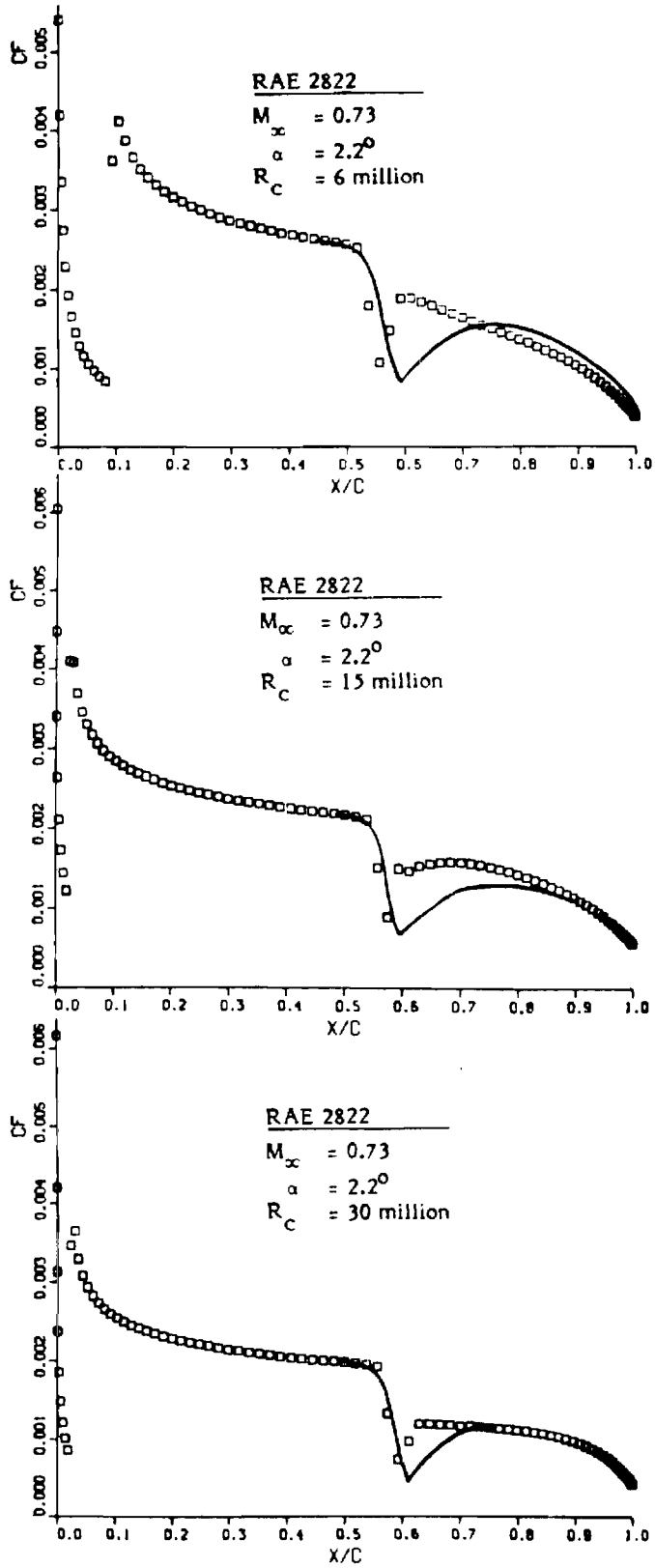

Figure 5. Variation of the skin friction coefficient with the SBLI theory (□□□) and without it (——)

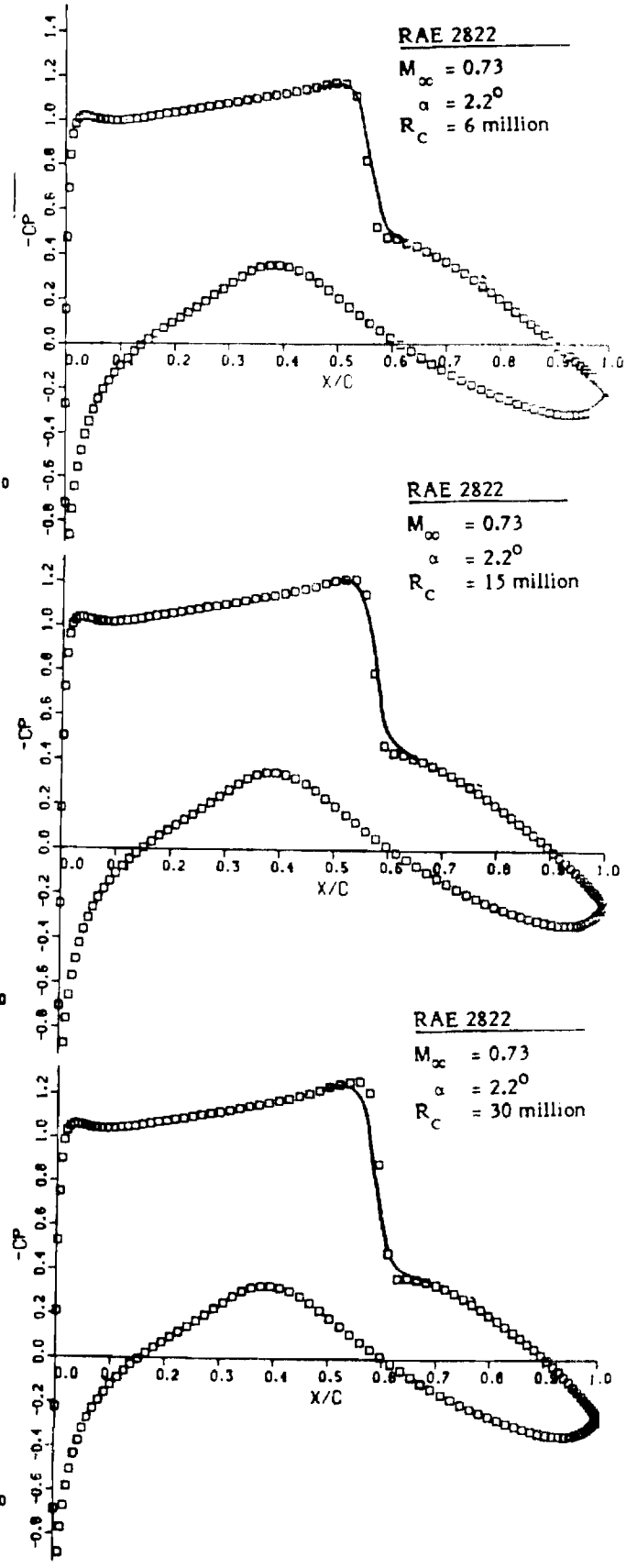

Figure 6. Variation of the pressure distribution with the SBLI theory (□□□) and without it (——)

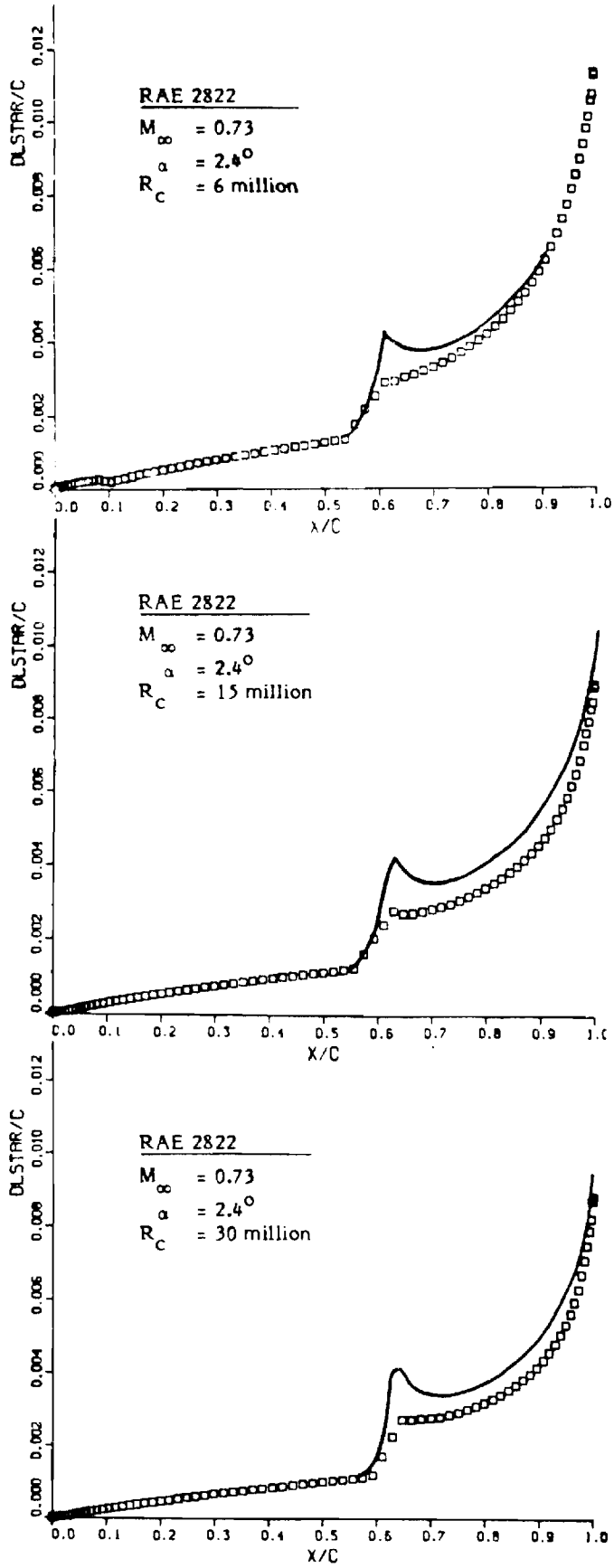

Figure 7. Variation of the displacement thickness with the SBLI theory (□□□) and without it (——)

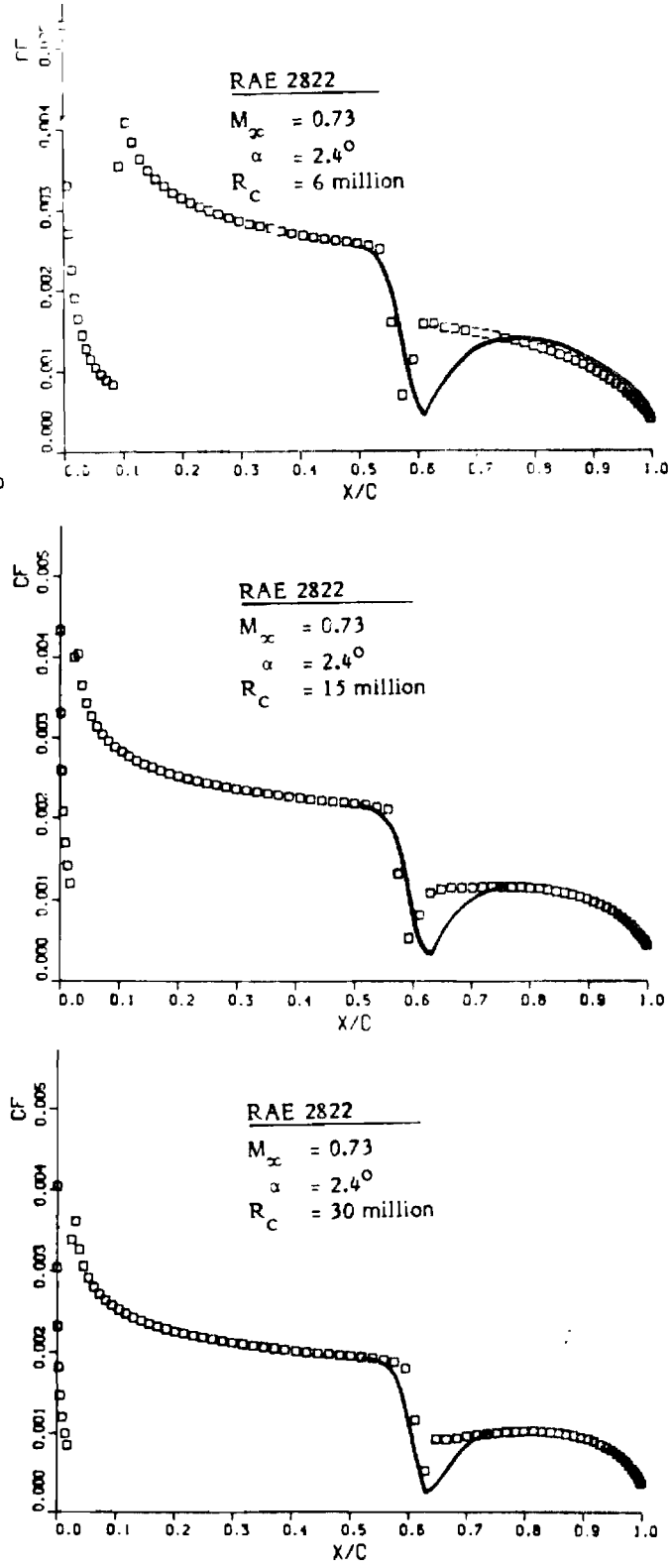

Figure 8. Variation of the skin friction coefficient with the SBLI theory (□□□) and without it (——).

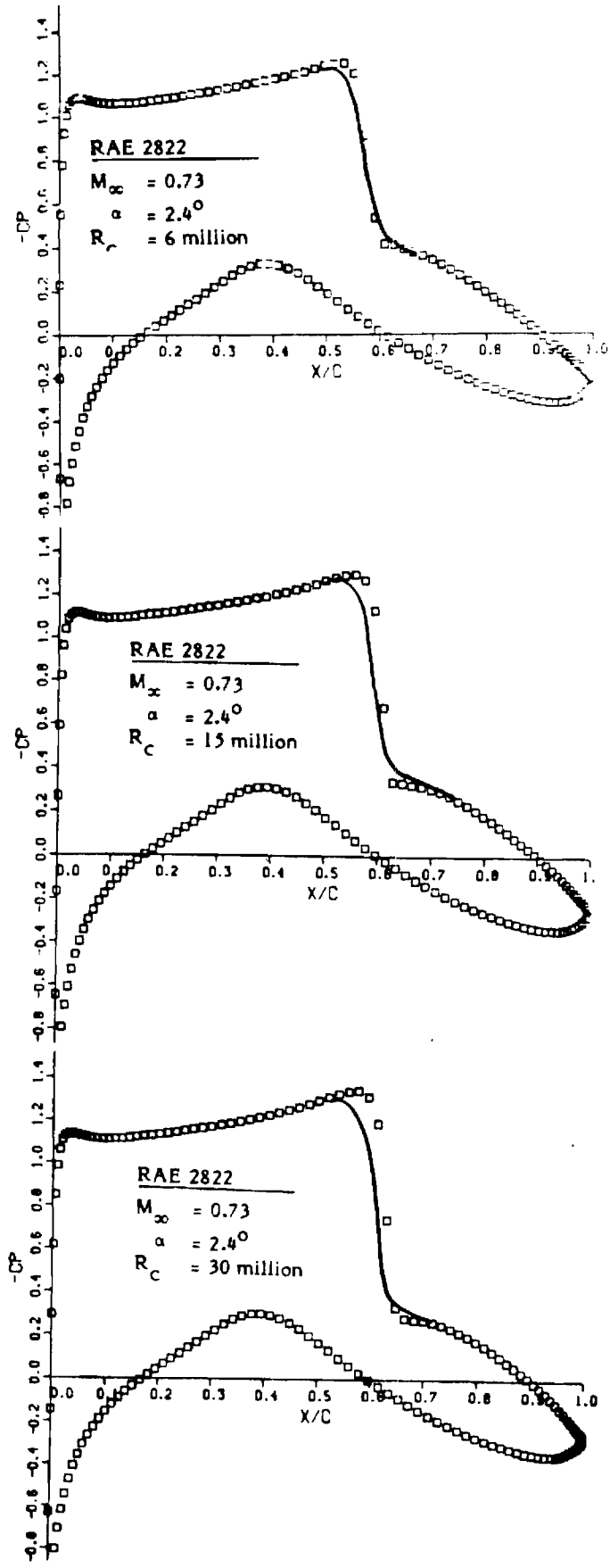

Figure 9. Pressure distribution with the SBLI theory (□□□) and without it (——)

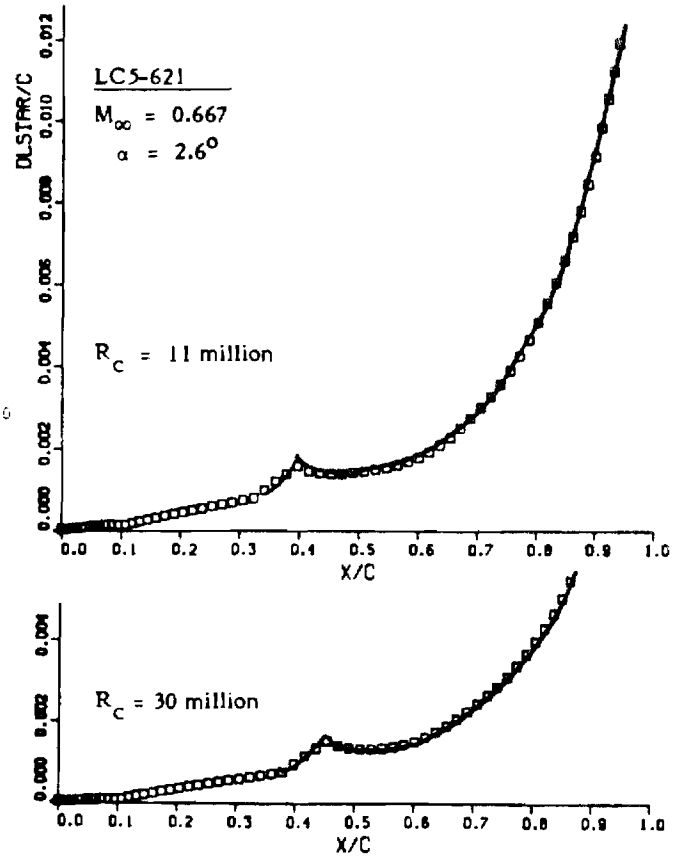

Figure 10. Variation of the displacement thickness with the SBLI theory (□□□) and without it (——)

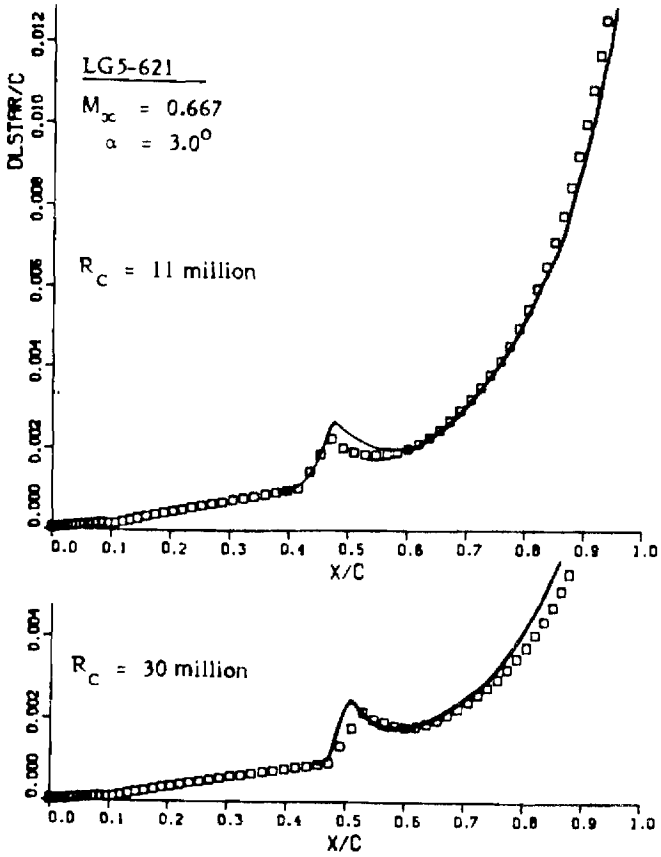

Figure 11. Variation of the displacement thickness with the SBLI theory (□□□) and without it (——)

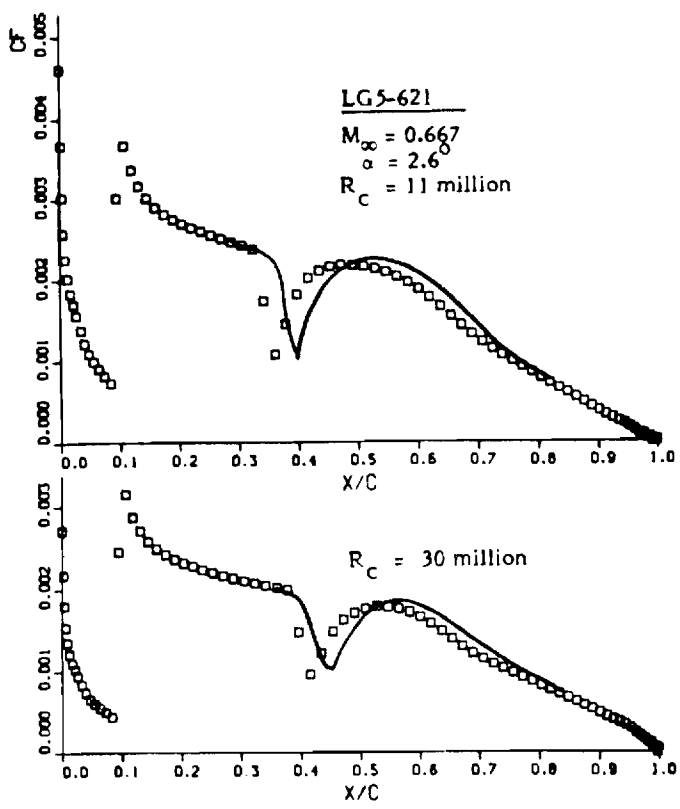

Figure 12. Variation of the skin friction coefficient with the SBLI theory (□□□) and without it (——)

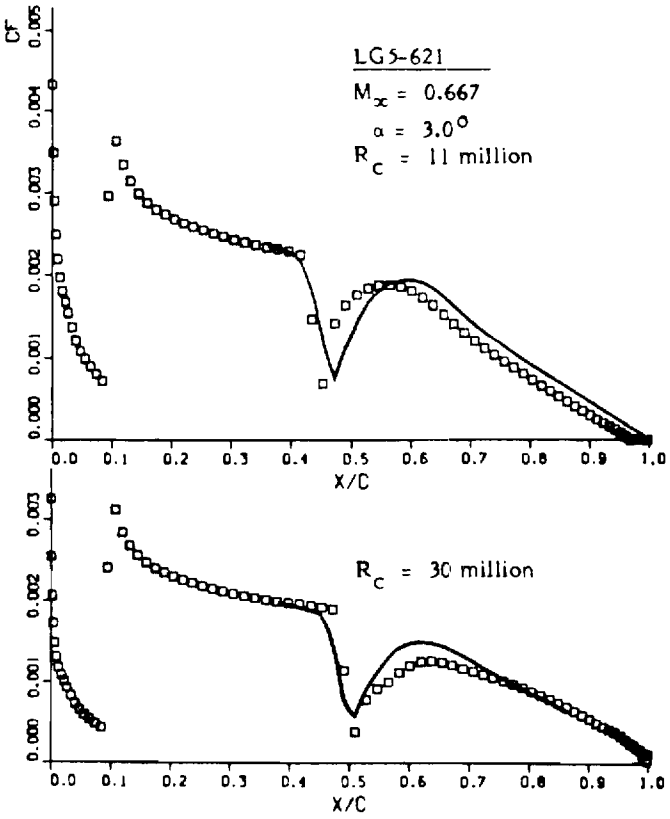

Figure 13. Variation of the skin friction coefficient with the SBLI theory (□□□) and without it (——)

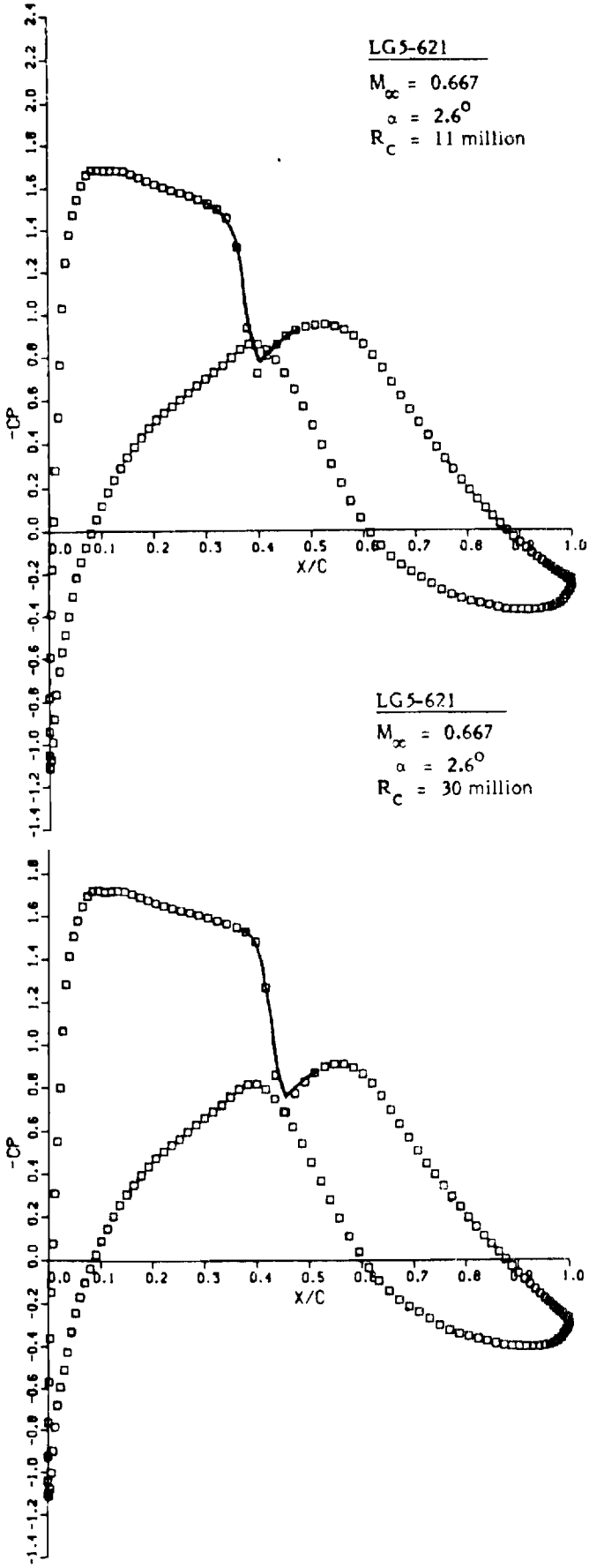

Figure 14. Variation of the pressure coefficient with the SBLI theory (□□□) and without it (——)

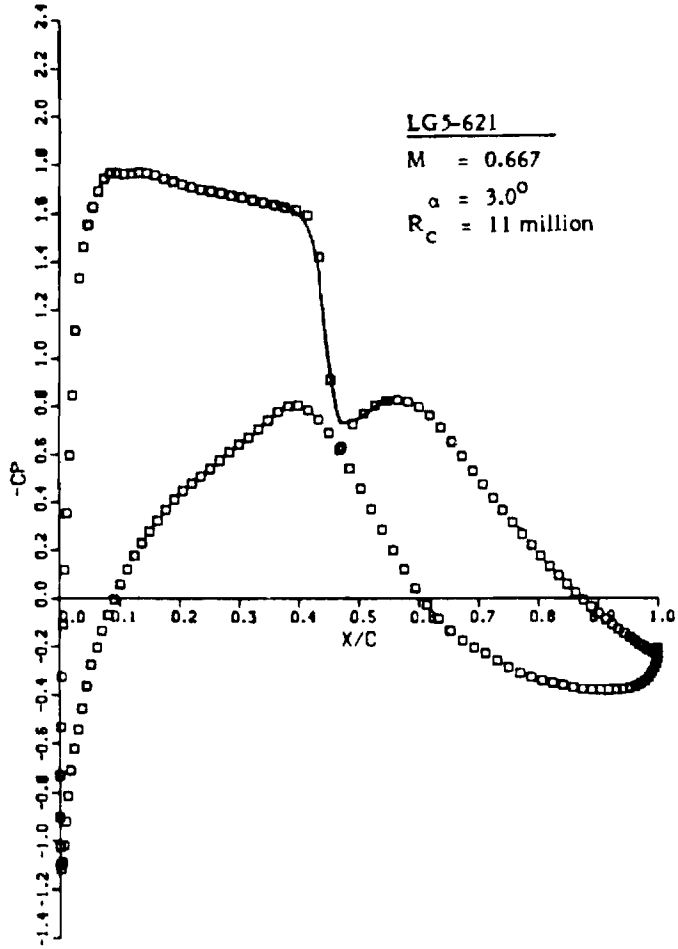

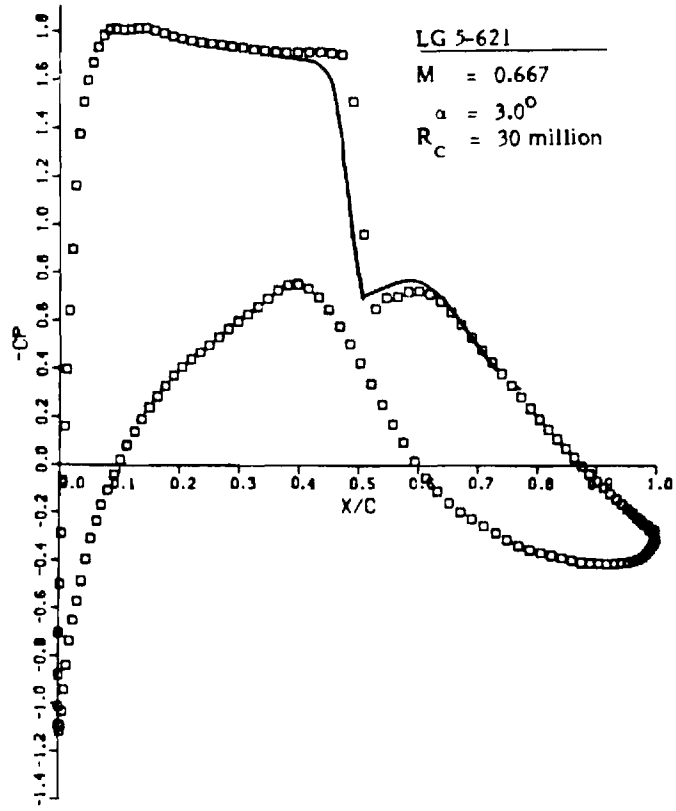

Figure 15. Variation of the pressure coefficient with the SBLI theory (□□□) and without it (——)

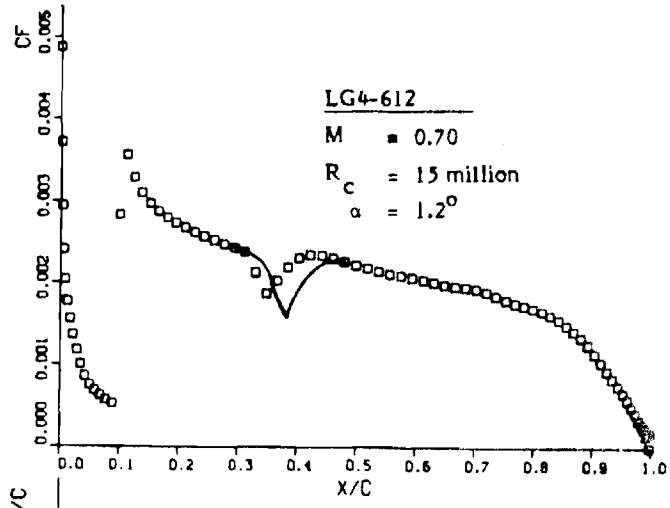

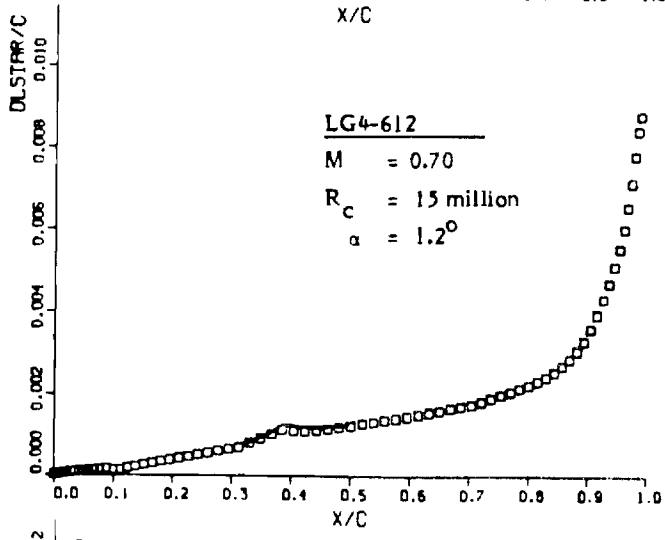

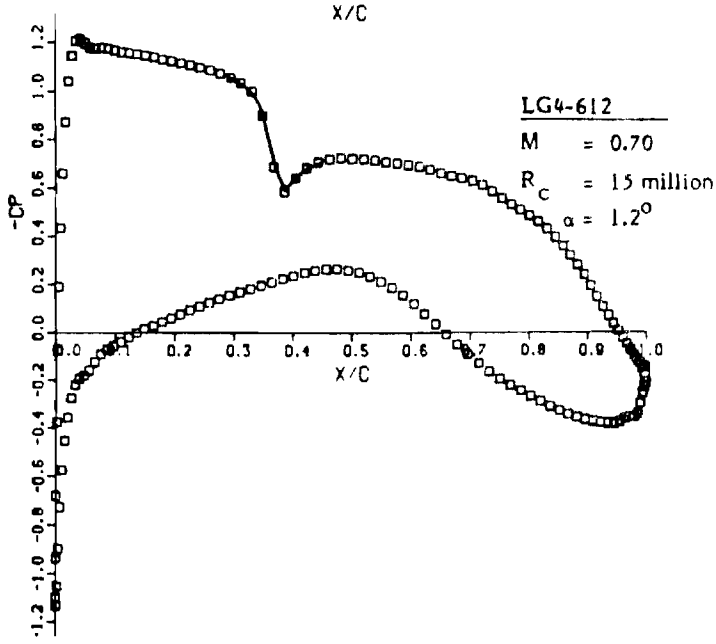

Figure 16. Results for the LG4-612 airfoil with SBLI (□□□) and without it (——)

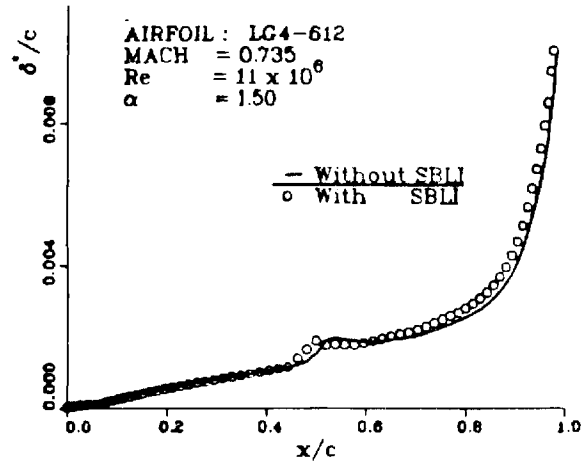

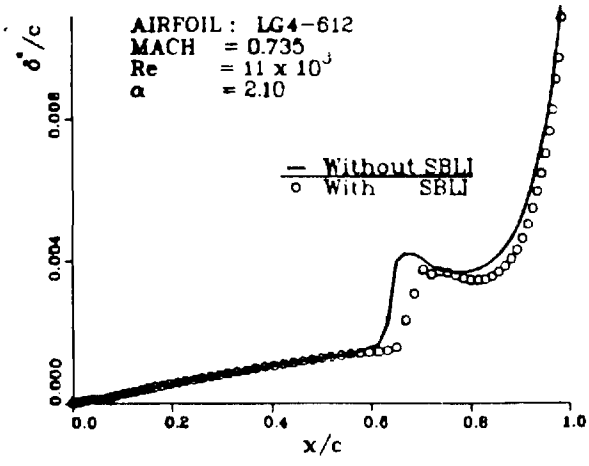

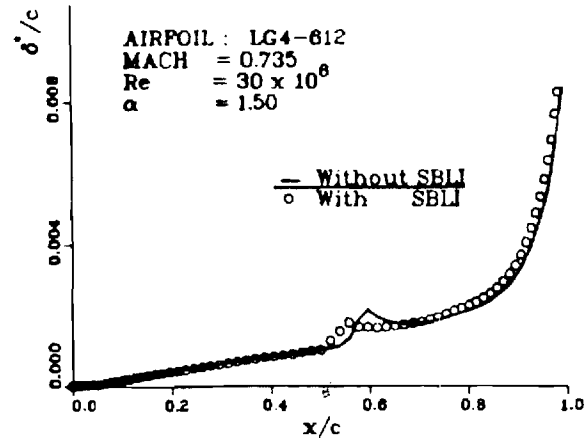

Figure 17. Upper surface displacement thickness

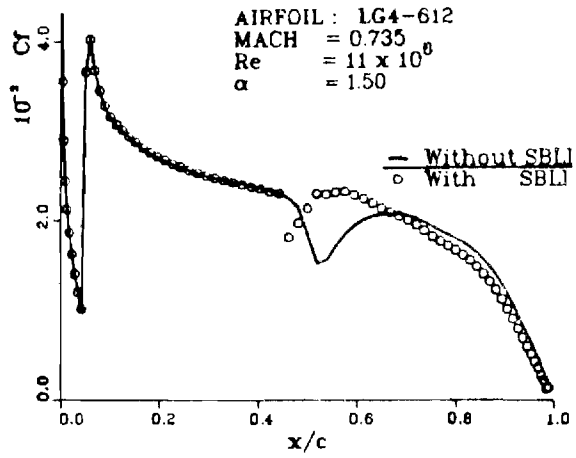

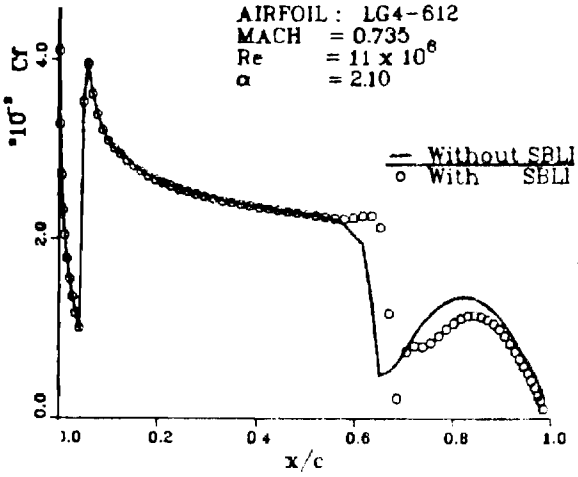

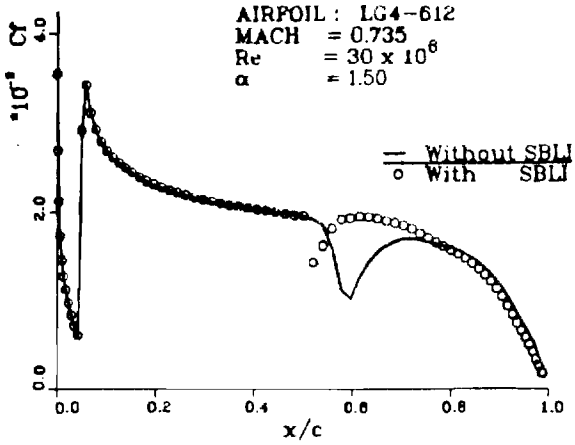

Figure 18. Upper surface skin friction coefficient

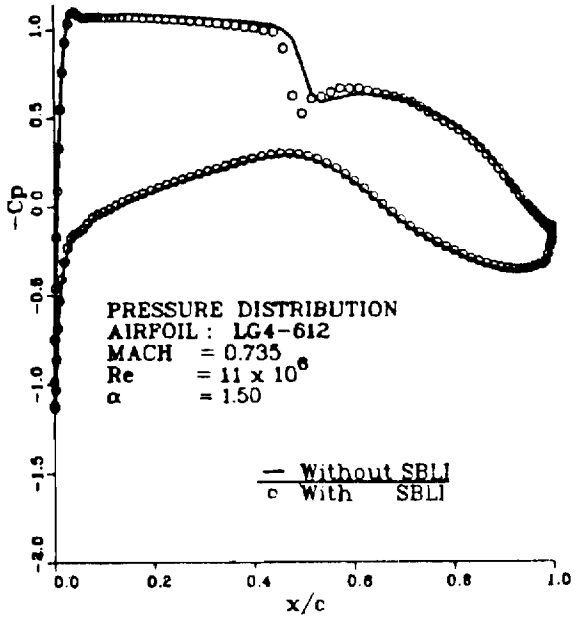

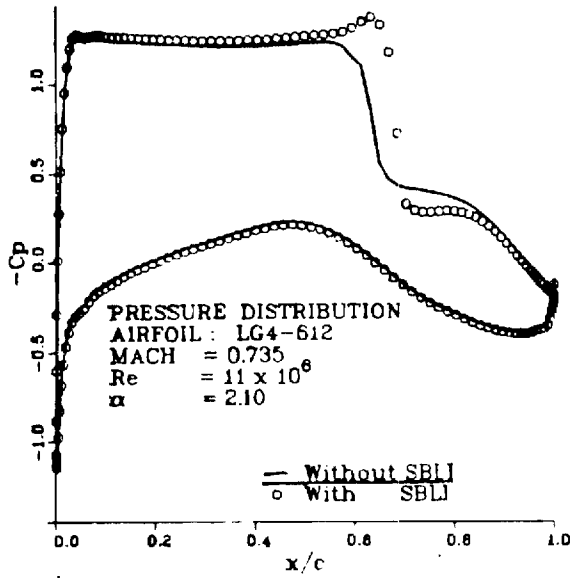

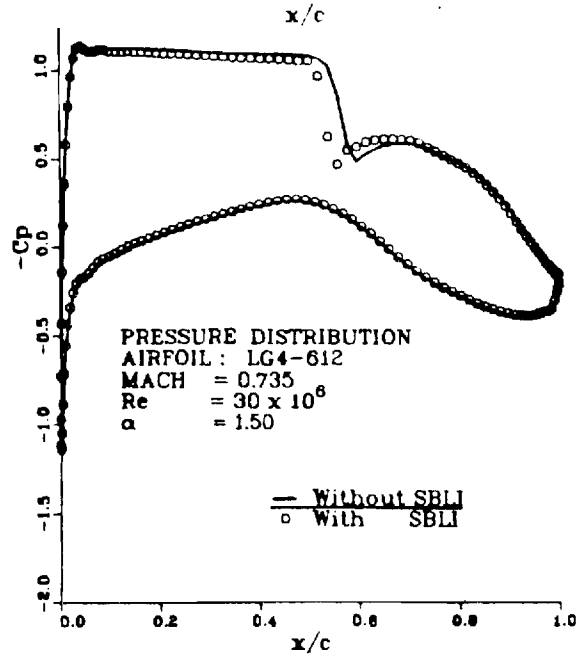

Figure 19. Pressure distribution

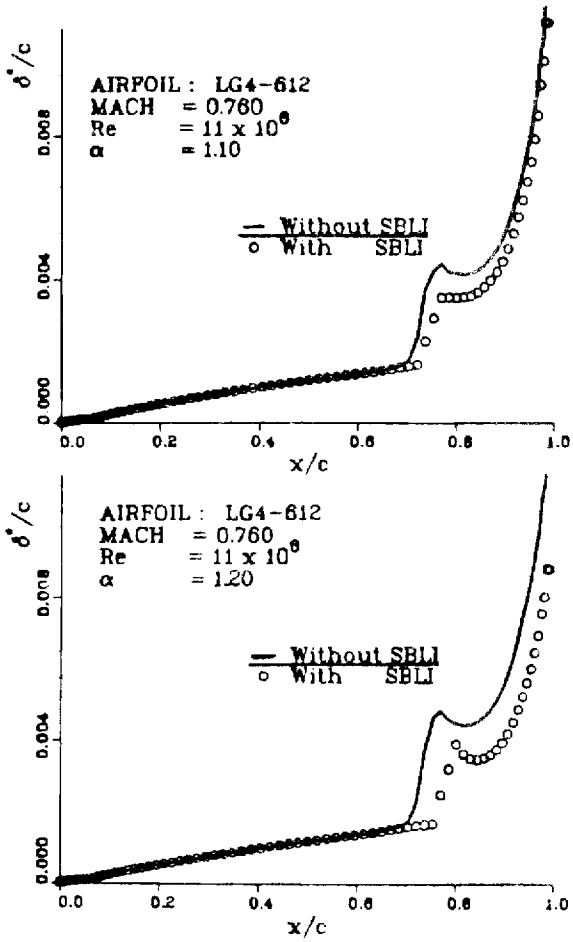

Figure 20. Upper surface displacement thickness

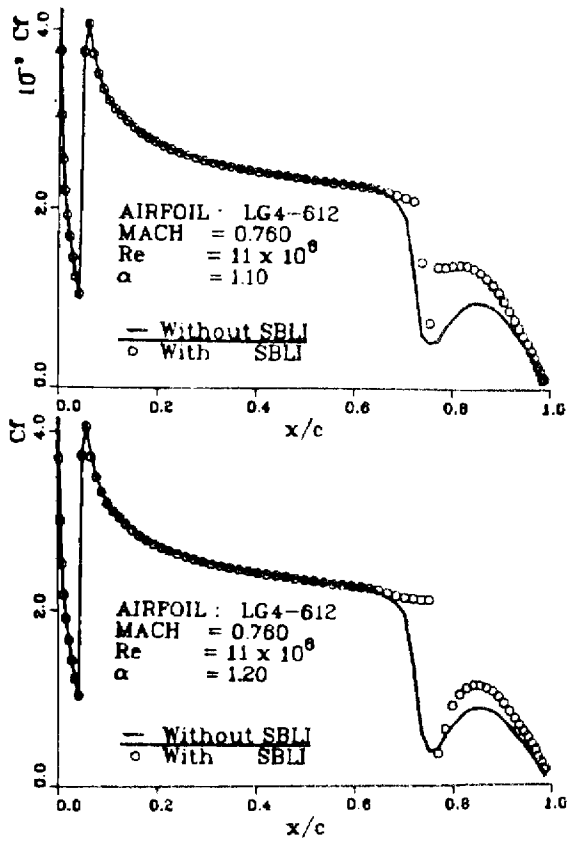

Figure 21. Upper surface skin friction distribution

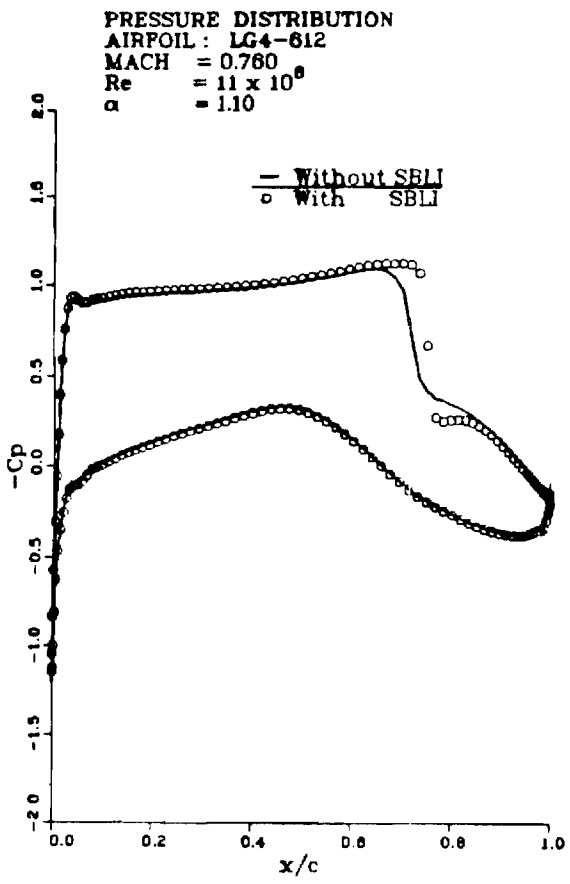

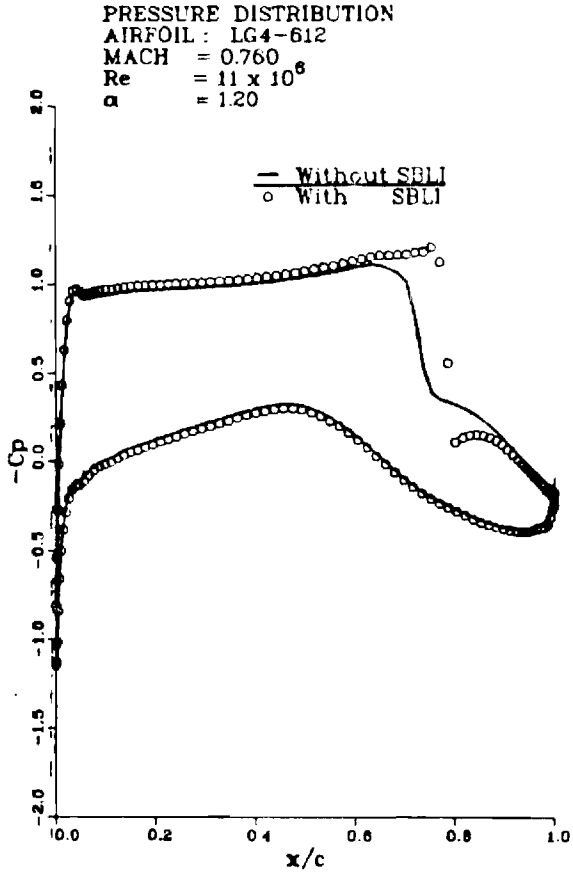

Figure 22. Pressure distribution

References

1. "Computation of Viscous/Inviscid Interactions," AGARD Conference Proceedings, No. 291, 1981.

2. Melnik, R.E., "Turbulent Interactions on Airfoils at Transonic Speeds - Recent Developments," Paper No. 10 in AGARD CP-291, 1981.

3. Ragab, S., and S.G. Lekoudis, "Validation of the GRUMFOIL Computer Code," Engineering Report, Lockheed-Georgia, 810093, May 1981.

4. Inger, G.R., "Transonic Shock-Turbulent Boundary Layer Interaction and Incipient Separation on Curved Surfaces", AIAA Paper 81-1244

5. Inger, G.R., "Some Features of a Shock-Turbulent Boundary Layer Interaction Theory in Transonic Flowfields", Paper No. 18 in AGARD CP-291, 1981.

6. Nandanan, M., Stanewsky, E. and Inger, G.R., "Airfoil Flow Analysis with a Special Solution for Shock/Boundary Layer Interaction," AIAA Journal, Vol. 19, No. 12, pp. 1540-1546, 1981.

7. Green, J.E., Weeks, D.J., and Brooman, J.W.F., "Prediction of Turbulent Boundary Layers and Wakes in Compressible Flow by a Lag-Entrainment Method", RAE Technical Report 72231, Dec. 1973.

8. Hinson, B.L., "High Reynolds Number Test of a 21-Percent Thick Supercritical Airfoil at Transonic Speeds", Lockheed-Georgia Report LG75ER0192, 1975.

9. Keable, F. and Smith, P.R., "High Reynolds Number Test of a 12-Percent Thick Supercritical Airfoil," Lockheed-Georgia Report LG5 ER0147, 1975.

APPENDIX B

AIAA'83

AIAA-83-0454

Boundary Layer Calculations in the Inverse Mode for Incompressible Flows Over Infinite Swept Wings

S. Radwan and S.G. Lekoudis, Georgia Institute of Technology, Atlanta, GA

AIAA 21st Aerospace Sciences Meeting

January 10-13, 1983/Reno, Nevada

BOUNDARY LAYER CALCULATIONS IN THE INVERSE MODE FOR INCOMPRESSIBLE FLOWS OVER INFINITE SWEPT WINGS

S. Radwan* and S. G. Lekoudis**
School of Aerospace Engineering
Georgia Institute of Technology
Atlanta, Georgia 30332

Abstract

The boundary layer equations for incompressible steady, turbulent flows are solved in the inverse mode under the infinite swept cylinder assumption. The Keller-box is used with weighted upwinding in order to suppress oscillations in the solution. An anisotropic eddy-viscosity formula is used for modeling the turbulence. The computed results are compared with measured data. The scheme allows marching into the region of three-dimensional separated flow.

1. Introduction

The computation of three-dimensional separated flows is of interest in several areas of applied aerodynamics. Three-dimensional separated flows occur on the unswept afterbodies of military transports, in regions of shock/boundary layer interactions, or on the upper surface of wings. These few flowfields are only part of a large number of flowfields around vehicles, where three-dimensional separated flows are present.

An arbitrary classification of ways of computing three-dimensional viscous flowfields is the following. One category consists of the methods that solve the three-dimensional Navier-Stokes equations for the whole field. In favor of this category is the increasing memory and speed of the available computers and, usually, the simplicity of coding as compared with the second category. The second category consists of methods that use different approximations to the Navier-Stokes equations for different parts of the flowfield and then combine the solutions. In its favor is the increased resolution available because of the segmentation of the flowfield, and, sometimes, the faster convergence in terms of total execution time. Moreover, related to the problem of the resolution is the decreased amount of artificial diffusion present, which increases the usefulness of the final answer. In spite of these advantages, the vast majority of the calculations that belong to the second category are done for attached three-dimensional flows.

If one attempts to use the second approach for computing three-dimensional separated flows, he has to decide on the equations that he will use in the area where the separation region originates on the body. This question, of what equations to use, has been asked many times before, and it is related to the singularity of the boundary layer equations when the pressure is prescribed. The appearance of the singularity does not necessarily mean that the validity of the boundary layer assumptions is lost. However it can be interpreted as an indication of separation. This is not always justifiable. An illuminating discussion about the subject is in the introduction of Reference 1. The singularity is avoided when the boundary layer equations are solved in the inverse mode.

Inverse boundary layer calculations for two-dimensional flows have been reported several times before in the literature. References 2 through 9 describe different methods that allow one to march into the separated region using prescribed displacement thickness or skin friction distributions. Also viscid/inviscid coupling procedures have been developed that include regions of separated flow. Such procedures are reported in References 10 through 17, and the capability of the schemes to numerically capture separated flow regions is demonstrated. Reference 18 includes a favorable comparison between full Navier-Stokes calculations and inverse boundary layer calculations. In spite of the number of the works performed for the two-dimensional case, it seems that the range of validity of the boundary layer calculations in the inverse mode is still judged by its convergence. Moreover the experience in the use of the inverse boundary layer calculations for three-dimensional separated flows is very limited.

To the authors' knowledge, Reference 1 contains the only available three-dimensional boundary layer calculations in the open literature, where the inverse mode is used.* In Reference 1 an integral method was used to solve the boundary layer equations. Some of the relative advantages and disadvantages of integral techniques versus finite-difference techniques for solving the boundary layer equations are as follows. The integral methods are faster and usually require less computer memory.

---

* Graduate Research Assistant, Student Member AIAA.

** Assistant Professor, Member AIAA.

* At the time this paper was written, Dr. Ragab of Lockheed-Georgia informed the authors of Reference 25.

Because a shape is assumed for the velocity profiles, it is difficult to examine relatively sophisticated turbulence models. Moreover higher order effects, like the variation of the pressure in the direction normal to the wall, or the effects of curvature, are difficult to incorporate. These effects seem to be important in regions close to separation as shown from measurements in both two and three-dimensional flows (References 19 and 20).

In this work, the three-dimensional boundary layer equations for laminar and turbulent flow are solved in the inverse mode under the ideal and approximate infinite yawed cylinder assumptions. The Keller-box is used with a modification that suppresses oscillations in the solution. The calculations are compared with the measurements reported in Reference 1, and the capability of the scheme to march into the separated flow region is demonstrated.

The analytical formulation and the turbulence model are described in Section 2, the numerical procedure is in Section 3 and the results are in the Section 4 of this paper.

2. The Analytical Formulation

2.1 The Governing Equations and the Boundary Conditions

The equations for three-dimensional boundary layers in steady, incompressible, turbulent flow over an infinite yawed cylinder, whose generator is parallel to the z-axis of an x, y, z cartesian coordinate system, shown in Figure 1, are:

$$\frac{\partial \overline{u^*}}{\partial x^*} + \frac{\partial \overline{v^*}}{\partial y^*} = 0 \qquad (1a)$$

$$\overline{u^*}\frac{\partial \overline{u^*}}{\partial x^*} + \overline{v^*}\frac{\partial \overline{u^*}}{\partial y^*} = -\frac{1}{\rho^*}\frac{\partial \overline{p^*}}{\partial x^*} + \frac{\partial}{\partial y^*}\left(\nu^*\frac{\partial \overline{u^*}}{\partial y^*} - \overline{u^{*\prime} v^{*\prime}}\right) \qquad (1b)$$

$$\overline{u^*}\frac{\partial \overline{w^*}}{\partial x^*} + \overline{v^*}\frac{\partial \overline{w^*}}{\partial y^*} = -\frac{1}{\rho^*}\frac{\partial p^*}{\partial z^*} + \frac{\partial}{\partial y^*}\left(\nu^*\frac{\partial \overline{w^*}}{\partial y^*} - \overline{w^{*\prime} v^{*\prime}}\right) \qquad (1c)$$

In equations (1), stars denote dimensional quantities, bars denote time-averages, primes denote fluctuating quantities, u, v, w are the velocity components in the x, y, z direction respectively, ρ is the density, p the pressure and ν the kinematic viscosity. Note that the term $-1/\rho\ \partial p/\partial z$ is retained in order to apply the infinite yawed cylinder conditions both in an ideal and in an approximate way.

We introduce an algebraic eddy-viscosity model for the Reynolds stresses (Reference 24),

$$-\overline{u^{*\prime} v^{*\prime}} = \nu^*\left[(b_1-1)\frac{\partial \overline{u^*}}{\partial y^*} + b_2\frac{\partial \overline{w^*}}{\partial y^*}\right] \qquad (2a)$$

$$-\overline{w^{*\prime} v^{*\prime}} = \nu^*\left[(b_3-1)\frac{\partial \overline{w^*}}{\partial y^*} + b_2\frac{\partial \overline{u^*}}{\partial y^*}\right] \qquad (2b)$$

When the equations are solved in the inverse mode we introduce the two component vector potential,

$$\psi^* = \sqrt{U_\infty^*\,\nu^*\,L^*}\ f(x,\eta) \qquad (3a)$$

$$\phi^* = \sqrt{U_\infty^*\,\nu^*\,L^*}\ g(x,\eta) \qquad (3b)$$

so that,

$$\overline{u^*} = \frac{\partial \psi^*}{\partial y^*},\quad \overline{w^*} = \frac{\partial \phi^*}{\partial y^*},\quad \overline{v^*} = -\left(\frac{\partial \psi^*}{\partial x^*} + \frac{\partial \phi^*}{\partial z^*}\right) \qquad (4a,b,c)$$

and the boundary-layer coordinates,

$$x = \frac{x^*}{L^*},\quad \eta = \frac{y^*}{L^*}\sqrt{R_L},\quad R_L = \frac{U^*L^*}{\nu^*} \qquad (5a,b,c)$$

with U_∞ and L being the reference velocity and length.

Then the thin shear layer equations become

$$(b_1 f'')' + \overline{U_e}\frac{d\overline{U_e}}{dx} = f'\frac{\partial f'}{\partial x} - f''\frac{\partial f}{\partial x} - (b_2 g'')' \qquad (6a)$$

$$(b_3 g'')' + \overline{U_e}\frac{d\overline{w_e}}{dx} = f'\frac{\partial g'}{\partial x} - g''\frac{\partial f}{\partial x} - (b_2 f'')' \qquad (6b)$$

In equations (6) primes denote derivatives with respect to η. The second term in (6b) is retained as an approximation to the nonzero $-1/\rho\ \partial p/\partial z$ term. This is possible by observing that the Euler equations at the boundary layer edge give

$$u_e^* \frac{\partial u_e^*}{\partial x^*} + w_e^* \frac{\partial u_e^*}{\partial z^*} = - \frac{1}{\rho^*} \frac{\partial p^*}{\partial x^*} \qquad (7a)$$

$$u_e^* \frac{\partial w_e^*}{\partial x^*} + w_e^* \frac{\partial w_e^*}{\partial z^*} = - \frac{1}{\rho^*} \frac{\partial p^*}{\partial z^*} \qquad (7b)$$

The equation (7b) without the second term of the left side is used to approximate a spanwise pressure gradient. This pressure gradient can be neglected in the calculations by using a flag in the input data.

The boundary conditions force the velocity to vanish at the wall which gives,

$$f = f' = g = g' = 0 \quad \text{at} \quad \eta = 0 \qquad (8a)$$

The displacement thicknesses

$$\delta_x^* = \int_0^\infty \left(1 - \frac{u^*}{u_e^*}\right) dy^* \qquad (8b)$$

$$\delta_z^* = \int_0^\infty \left(1 - \frac{w^*}{w_e^*}\right) dy^* \qquad (8c)$$

are prescribed functions of x^*. The six conditions (8) are used as boundary conditions in order to solve the system of equations (6) numerically.

The initial conditions for the inverse calculations can be generated in several ways. The experimental velocity profiles can be used, or velocity profiles formed by polynomial expressions, or solutions of the boundary layer equations in the direct mode can also be used. The last procedure was followed in this work. Therefore, the equations were also solved in the direct mode. The two-component vector potential used in this case is

$$\psi^* = \sqrt{u_e^* \nu^* x^*}\, f(x,\eta) \qquad (9a)$$

$$\phi^* = \sqrt{u_e^* \nu^* x^*}\, g(x,\eta) w_e^*/u_e^* \qquad (9b)$$

The velocities are still given by equations (4) but the boundary layer coordinates are

$$x = \frac{x^*}{L^*}, \quad \eta = \frac{y^*}{x^*}\sqrt{R_x}, \quad R_x = \frac{u_e^* x}{\nu^*} \qquad (10a,b,c)$$

Then the thin shear layer equations (1) become

$$(b_1 f'')' + \tfrac{1}{2}(1 + p_2) f'' f + p_2 (1 - f'^2) = x\left(f' \frac{\partial f'}{\partial x} - f'' \frac{\partial f}{\partial x}\right) - (b_2 g'')' \, w_e/u_e \qquad (11a)$$

$$(b_3 g'')' + \tfrac{1}{2}(1 + p_2) f g'' + p_3 (1 - g' f') = x\left(f'' \frac{\partial g'}{\partial x} - g'' \frac{\partial f}{\partial x}\right) - (b_2 f'')' \, u_e/w_e \qquad (11b)$$

where

$$p_2 = \frac{x^*}{u_e^*} \frac{du_e^*}{dx^*} \qquad (12a)$$

$$p_3 = \frac{x^*}{w_e^*} \frac{dw_e^*}{dx^*} \qquad (12b)$$

The boundary conditions for the system (11) are:

$$f = f' = g = g' = 0 \quad \text{at } \eta = 0 \qquad (13a)$$

$$f' = g' = 1 \quad \text{at } \eta = \eta_e \qquad (13b)$$

2.2 The Turbulence Model

The anisotropic eddy-viscosity model suggested by Rotta (Paper 24) is used. It is an algebraic eddy-viscosity model with

$$\varepsilon_i^* = L^{*2} \left[\left(\frac{\partial u^*}{\partial y^*}\right)^2 + \left(\frac{\partial w^*}{\partial y^*}\right)^2 + (T-1) \frac{\left(w^* \frac{\partial u^*}{\partial y^*} - u^* \frac{\partial w^*}{\partial y^*}\right)^2}{u^{*2} + w^{*2}} \right] \qquad (14a)$$

$$\varepsilon_o^* = 0.0168 \left| \int_0^\infty \left[(u_e^{*2} + w_e^{*2})^{\frac{1}{2}} - (u^{*2} + w^{*2})^{\frac{1}{2}} \right] dy^* \right| \qquad (14b)$$

$$b_1 = \frac{\varepsilon^*}{\nu^*} (u^{*2} + T w^{*2})/(u^{*2} + w^{*2}) \qquad (14c)$$

$$b_2 = \frac{\varepsilon^*}{\nu^*} (1 - T) u^* w^*/(u^{*2} + w^{*2}) \qquad (14d)$$

$$b_3 = \frac{\varepsilon^*}{\nu^*} (w^{*2} + T u^{*2})/(u^{*2} + w^{*2}) \qquad (14e)$$

where ϵ^* is the turbulent viscosity and the subscripts i and o indicate inner and outer regions. They are determined numerically so that at their common boundary $\epsilon_i = \epsilon_o$. The mixing length L is defined using the Cebeci-Smith model (Reference 22). The parameter T, controlled from the input, changes the amount of anisotropy in the inner part of the boundary layer.

3. The Numerical Procedure

A code that solves the incompressible two-dimensional turbulent boundary layer equations in the inverse mode is available in Reference 22. We run the code, with modifications, for several test cases. It was found that, sometimes, oscillatory skin friction coefficients resulted from the converged solution. The same type of oscillations occurred for the case of three-dimensional flow. In order to eliminate these oscillations we modified the numerical scheme. The effect of the truncation error was controlled by computing with several grids.

The following dependent variables are used:

$$f = F_1 \qquad g = F_2 \tag{14a}$$

$$f' = U_1 \qquad g' = U_2 \tag{14b}$$

$$f'' = V_1 \qquad g'' = V_2 \tag{14c}$$

$$f_e' = W_1 \qquad g_e' = W_2 \tag{14d}$$

The system of equations (6) can then be rewritten in the form

$$F_1' = U_1 \tag{15a}$$

$$U_1' = V_1 \tag{15b}$$

$$(bV_1)' = -W_1 \frac{\partial W_1}{\partial x} + U_1 \frac{\partial U_1}{\partial x} - V_1 \frac{\partial F_1}{\partial x} - (b_2 V_2)' \tag{15c}$$

$$W_1' = p_1(\eta, x) \tag{15d}$$

$$F_2' = U_2 \tag{16a}$$

$$U_2' = V_2 \tag{16b}$$

$$(bV_2)' = -W_1 \frac{\partial W_2}{\partial x} + U_1 \frac{\partial U_2}{\partial x} - V_2 \frac{\partial F_1}{\partial x} - (b_2 V_1)' \tag{16c}$$

$$W_2' = p_2(\eta, x) \tag{16d}$$

The functions $p_1(\eta, x)$ and $p_2(\eta, x)$ can be prescribed from considerations of the variation of the pressure across the boundary layer. However in the results reported in this study, they are set equal to zero.

The equations (15) and (16) are coupled because b is a function of U_1, V_1, U_2, V_2. This happens even under the ideal swept cylinder assumption. Then the first term on the right side of equation (16c) is identically zero. The equations are uncoupled only for the case of laminar flow. The system of equations (16) is linear, provided the quantities with subscript 1, and the b's are known.

The solution procedure is based on the Keller-box scheme (References 6, 7, 22). The system of equations (15) is linearized and a Newton iteration is used together with an inversion of a block tridiagonal matrix. The element matrices are 4 x 4 square matrices. Then the system of equations (16) is solved without any linearization since it is already linear for the quantities with subscript 2. The same solver is used to invert the block tridiagonal matrix.

Note that the full three-dimensional problem involves two extra steps in the solution procedure. The first step is the inclusion of the extra terms on the right side of equations (15) and (16). The second step which is optional, is the use of the Newton's linearization in the equations (16). The solver remains identical. Such calculations will be reported in the future.

The variation of the box scheme that suppresses the oscillations in the skin friction coefficient works as follows. If we call B the station where the boundary layer quantities are known, C the station before it and A the station we are solving for, the Keller-box centers using the midpoint between A and B. In the original scheme only quantities at A and B are used. In this scheme the quantities q at B are replaced by

$$q_B = r\, q_C + (1 - r)\, q_B \tag{17}$$

where r is an upwinding parameter between zero and one. Equation (17) makes the scheme formally first order accurate and a three-point scheme in the marching direction.

In the reversed flow region the Reyhner and Flügge-Lotz approximation is used in two ways. Either U_1 is set equal to zero, or its negative is used, whenever U_1 itself is negative. The results are practically insensitive to the choice made.

4. Results and Discussion

We computed two-dimensional separated, turbulent, boundary layer flows in order to compare with measured data. The computed and measured freestream velocity profiles and skin friction coefficients are shown in Figures 2 through 5. The measurements shown in Figures 2 and 3 are from Reference 19 and the ones shown in Figures 4 and 5 are from the paper of Chu and Young in Reference 16. The initial profiles are generated by computing in the direct mode and obtaining a velocity profile that has skin friction coefficient and displacement thickness close to the ones measured in the most upwind station. In order to achieve that an effective origin for the x-axis is chosen for the data of Reference 19. The measurements were done on the tunnel wall. In both sets of measurements the separated turbulent boundary layer does not reattach. Thus, the measured data resemble separations that could occur on the upper surface of airfoils. The measured displacement thicknesses are interpolated using a cubic spline. The calculations predict the separation and reproduce the measured freestream velocities and skin friction with reasonable accuracy.

In order to examine the validity of the calculations for the three-dimensional boundary layer case, the displacement thicknesses computed in the direct mode were used as input for the calculations in the inverse mode. Table 1 shows the comparison between the computed freestream velocities and skin friction coefficients for the case of laminar flow and Table 2 shows it for turbulent flow. Reasonable agreement is obtained.

The experience gained from these calculations suggests that the initial profile is very important. A small mismatch between the profile's displacement thickness and the measured displacement thickness downstream, results in severe oscillations in the solution. Therefore effort was devoted to obtain initial profiles for the data of Reference 21. These data are for a separating turbulent boundary layer under conditions that correspond closely to the infinite swept wing conditions.

The measured velocity distribution at the boundary layer edge, with the anisotropy parameter T set equal to one, is used to compute the results shown in Figures 6 through 9. The computed quantities grossly misrepresent the development of the boundary layer. This is in agreement with previous calculations (Paper 16 of Reference 23). However, at the beginning of the measuring stations, numbered 1 through 10 in Reference 21, the computed boundary layer properties agree with the measured properties reasonably well, except for the displacement thicknesses (as defined in Reference 21).

Because of the discussed disagreement of the measured and computed displacement thicknesses at the beginning of the measuring stations, when the direct mode is used, the following procedure is followed. The displacement thicknesses used in the calculations with the inverse mode, shown in Figures 10 and 11, are slightly different than the measured ones at the first two stations. As shown in Figures 12 through 18 the initial boundary layer properties agree reasonably well with the measurements, as was the case with the direct mode. It is also shown in these Figures that the computations reproduce the measured growth of the boundary layer, including the separation. The separation location was computed without any difficulty. The differences between certain computed quantities created by the $\partial p/\partial z$ term in the equations is confined to the skin friction and edge velocities in the z-direction. In Figures 17 and 18 it is shown that the calculations reliably reproduced the measured turbulent velocity profile <u>inside</u> the separated region. This is the main accomplishment of the developed procedure. The variation of the anisotropy parameter T produced differences in the results with a tendency of moving the separation point upstream when T was decreased from unity. The calculation with T=1 predicted the separation closer to its measured location than T 1. The upwinding parameter r used in these calculations is r = .12.

In conclusion, the inverse mode is used to compute turbulent boundary layers under the infinite swept cylinder assumption. The scheme reproduces with reasonable accuracy measured data, including the region of three-dimensional separation.

In all the Figures the results [illegible] are for the case of isotropic eddy viscocity and the darkened symbol denote the measured data.

Acknowledgements

This work was supported by a grant from the Advanced Research Organization of the Lockheed-Georgia Company.

5. References

1. Cousteix, J. and Houdeville, R, "Singularities in Three-Dimensional Turbulent Boundary-Layer Calculations and Separation Phenomena", AIAA Journal, Vol. 19, No. 8, pp. 976-985, 1981.

2. Catherall, D. and Mangler, K.W., "The Integration of Two-Dimensional Laminar Boundary Layer Equations Past the Point of Vanishing Skin Friction," J. Fluid Mech., Vol. 26, Pt. 1, pp. 163-182, 1966.

3. Klineberg, J.M. and Steger, J.L., "On Laminar Boundary-Layer Separation," AIAA Paper No. 74-94, 1974.

4. Carter, J.E., "Inverse Boundary-Layer Theory and Comparison with Experiment," NASA TP-1208, 1978.

5. Carter, J.E. and Wornom, S.F., "Forward Marching Procedure for Separated Boundary-Layer Flows," AIAA Journal, Vol. 13, No. 8, pp. 1101-1103, 1975.

6. Cebeci, T., "An Inverse Boundary-Layer Method for Compressible Laminar and Turbulent Boundary Layers", J. Aircraft, Vol. 13, No. 9, 1976.

7. Cebeci, T., Keller, H.B. and Williams, P.G., "Separating Boundary-Layer Flow Calculations," J. of Computational Physics, Vol. 31, pp. 363-378, 1979.

8. Pletcher, R.H., "Prediction of Incompressible Turbulent Separating Flow," J. Fluids Engineering, Vol. 100, pp. 427-433, 1978.

9. Horton, H.P., "Comparisons Between Inverse Boundary-Layer Calculations and Detailed Measurements in Laminar Separated Flows," The Aeronautical Quarterly, Vol. XXXII, Pt. 3, pp. 169-187, 1981.

10. Carter, J.E., "Viscous-Inviscid Interaction Analyses of Transonic Turbulent Separated Flow", AIAA Paper 81-1241.

11. Gordon, R. and Rom, J., "Transonic Viscous-Inviscid Interaction Over Airfoils for Separated Laminar on Turbulent Flows," AIAA Journal, Vol. 19, No. 5, pp. 545-552, 1981.

12. Wigton, L.B. and Holt, M., "Viscous-Inviscid Interaction in Transonic Flow", AIAA Paper 81-1003.

13. Vatsa, V.N., Werle, M.J. and Verdon, J.M., "Viscid/Inviscid Interaction at Laminar and Turbulent Symmetric Trailing Edges," AIAA paper 82-0165.

14. Whitfield, D.L., Swafford, T.W. and Jacobs, J.L., "Calculation of Turbulent Boundary Layers with Separation and Viscous/Inviscid Interaction," AIAA Journal, Vol. 19, No. 10, pp.1315-1322, 1981.

15. Carter, J., "A New Boundary-Layer Inviscid Interaction Technique for Separated Flow", AIAA Paper 79-1450.

16. "Flow Separation", AGARD Conference Proceedings, No 168, 1975.

17. Ragab, S., Ph.D. Dissertation, Virginia Tech, 1979.

18. Johnson, D.A., Horstman, C.C. and Bachalo, W.D., "Comparison Between Experiment and Prediction for Transonic Turbulent Separated Flow," AIAA Journal, Vol. 20, No. 6, pp. 737-744, 1982.

19. Simpson, R.L., Chew, Y.T. and Shiraprassad, B.G., "The Structure of a Separating Turbulent Boundary Layer", Parts 1, 2, and 3, J. Fluid Mechanics, Vol. 113, pp. 23-91, 1981.

20. Ramaprian, B.R., Patel, V.C. and Choi, D.H., "Mean Flow Measurements in the Three-Dimensional Boundary Layer Over a Body of Revolution at Incidence," J. Fluid Mechanics, Vol. 103, pp. 479-504, 1981.

21. Van Den Berg, B., Elsenaar, A., Lindhout, J.P.F., and Wesseling, P., "Measurements in an Incompressible Three-Dimensional Turbulent Boundary Layer Under Infinite Swept Wing Conditions and Comparison with Theory," J. Fluid Mechanics, Vol. 70, p. 127, 1975.

22. Bradshaw, P., Cebeci, T. and Whitelaw, J., Engineering Calculation Methods for Turbulent Flow, Academic Press, 1981.

23. "Turbulent Boundary Layers: Experiments, Theory and Modeling", AGARD Conference Proceedings, No. 271, 1980.

24. Rotta, J.C., "A Family of Turbulence Models for Three-Dimensional Boundary Layers", Proceedings of 1st Symposium on Turbulent Shear Flows, Vol. I, 1977.

25. Formery, M. and Délery, J., "Méthode aux difference finies pur le calcul en mode inverse de la couche limite turbulente tridimensionnelle" La Recherche Aérospaciale, Année, No. 5 pp. 303-313, (Septembre-Octobre) 1981.

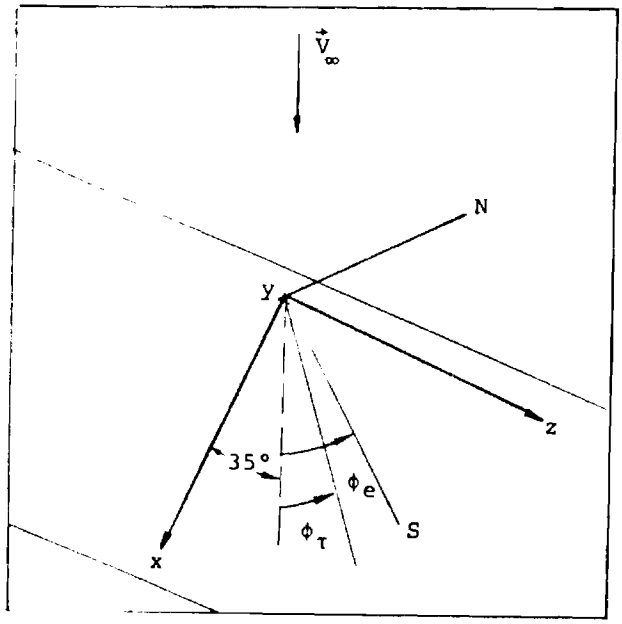

Figure 1. The coordinate system

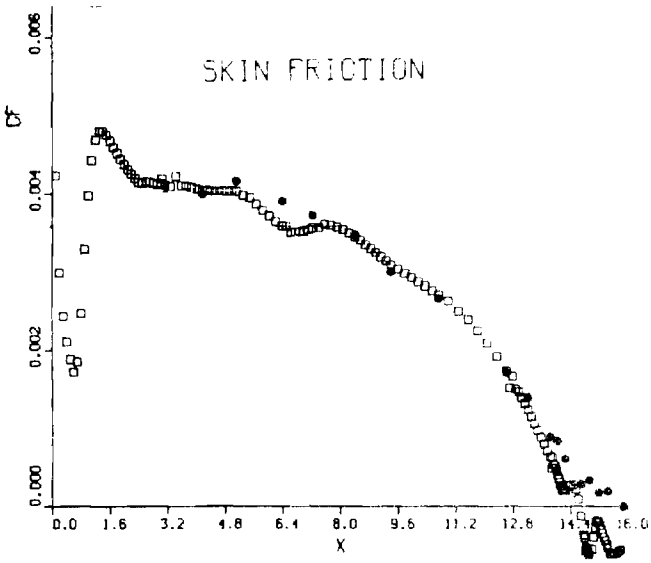

Figure 3. Comparison of computed and measured skin friction coefficients for the data of Reference 19.

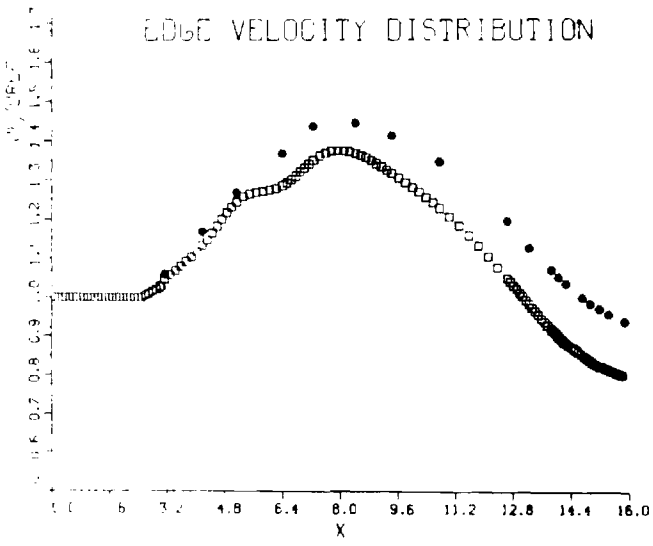

Figure 2. Comparison of computed and measured edge velocities for the data of Reference 19.

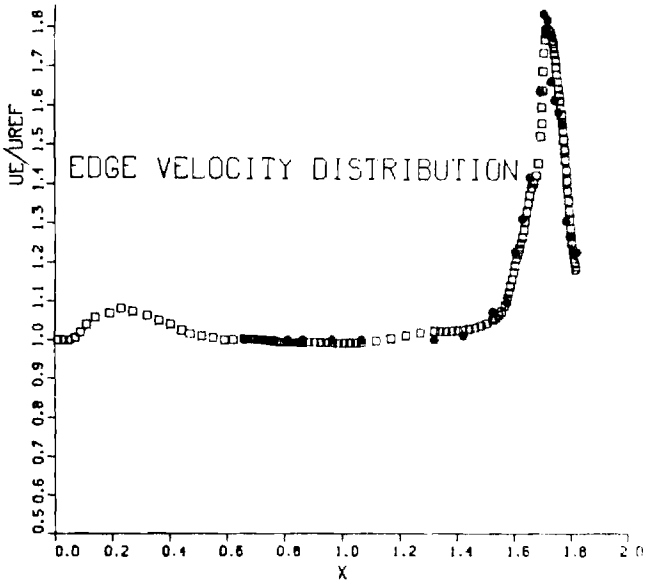

Figure 4. Comparison of computed and measured edge velocities for the data from the paper by Chu and Young in Reference 16.

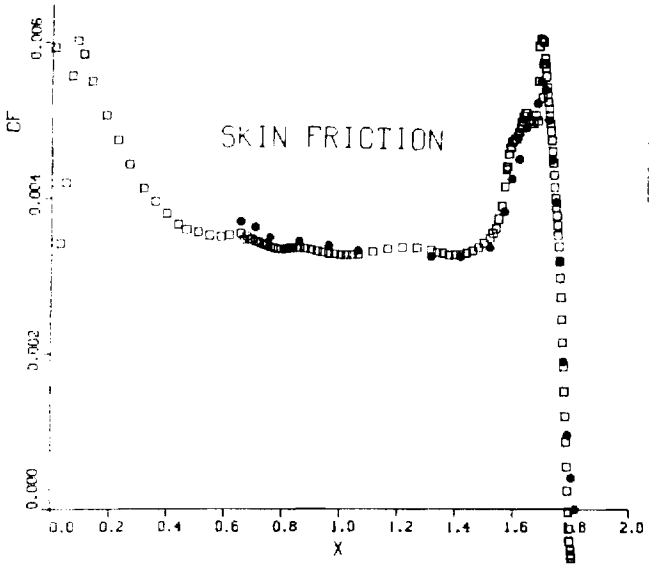

Figure 5. Comparison of computed and measured skin friction coefficients for the data from the paper by Chu and Young in Reference 16.

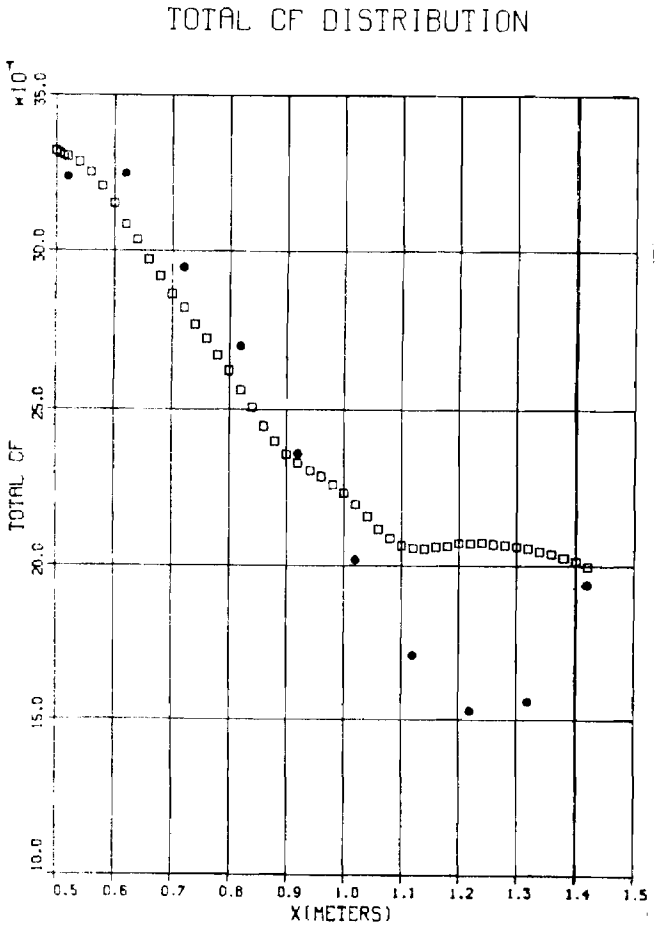

Figure 6. Calculations in the direct mode and comparison with measurements.

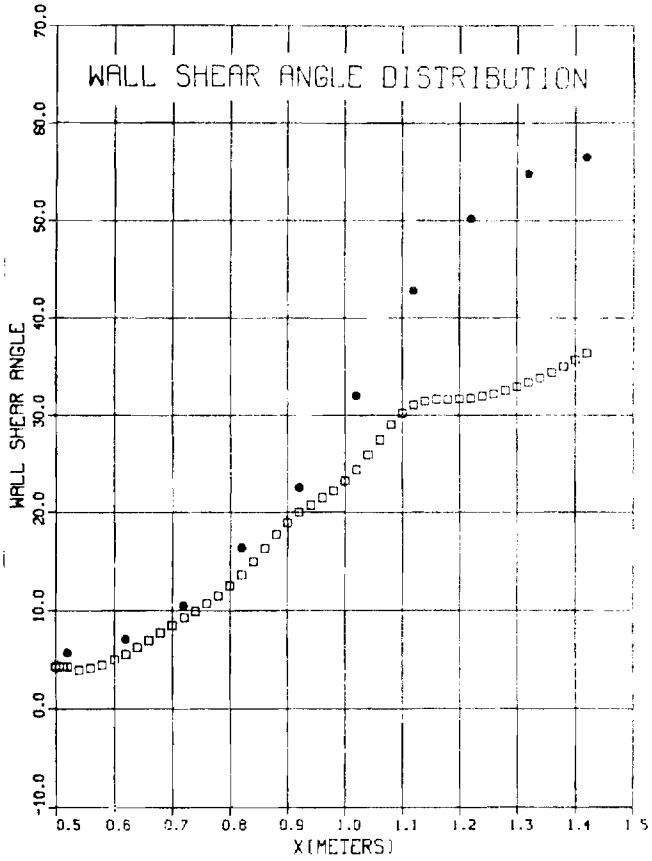

Figure 7. Calculations in the direct mode and comparison with measurements.

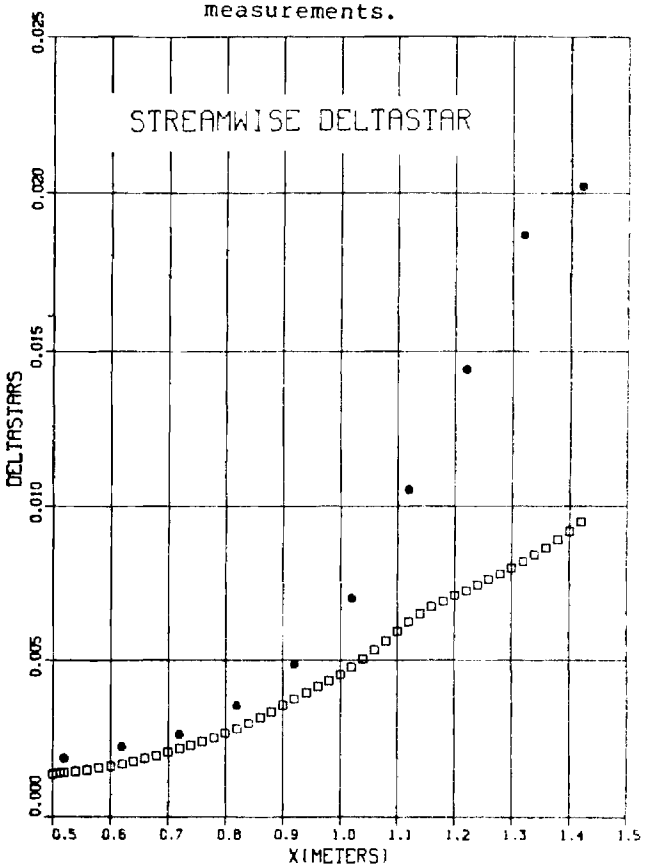

Figure 8. Calculations in the direct mode and comparison with measurements.

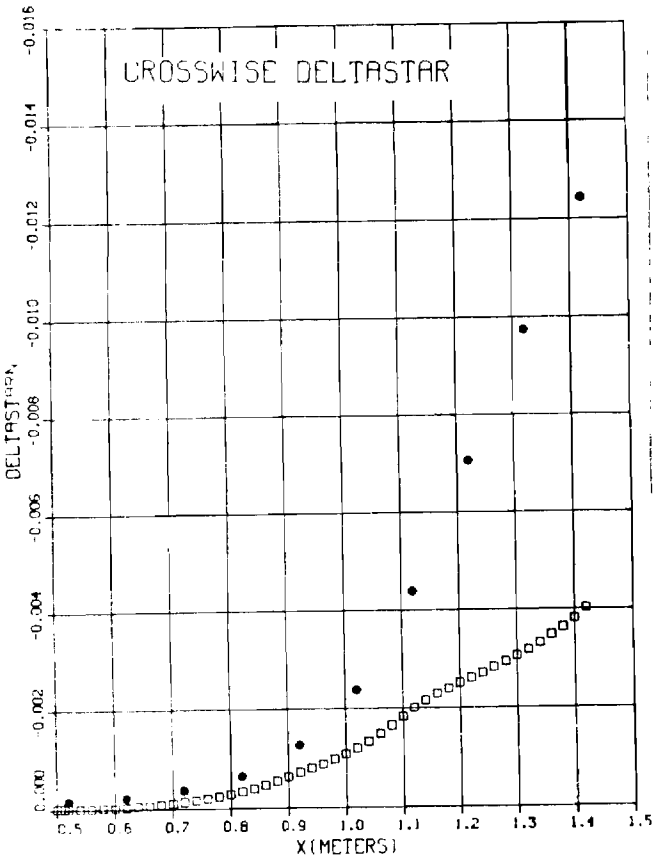

Figure 9. Calculations in the direct mode and comparison with measurements.

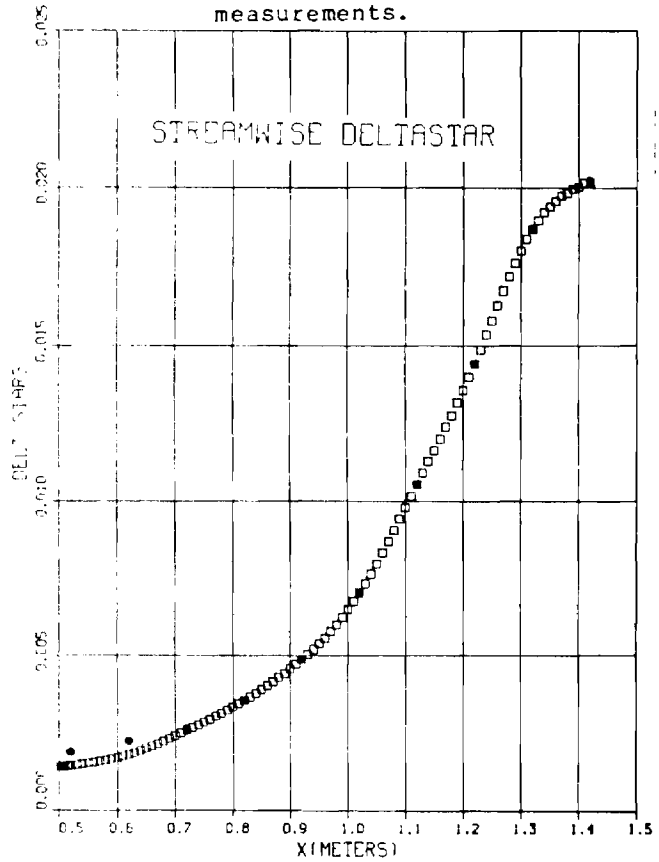

Figure 10. Displacement thickness used in the calculations with the inverse mode.

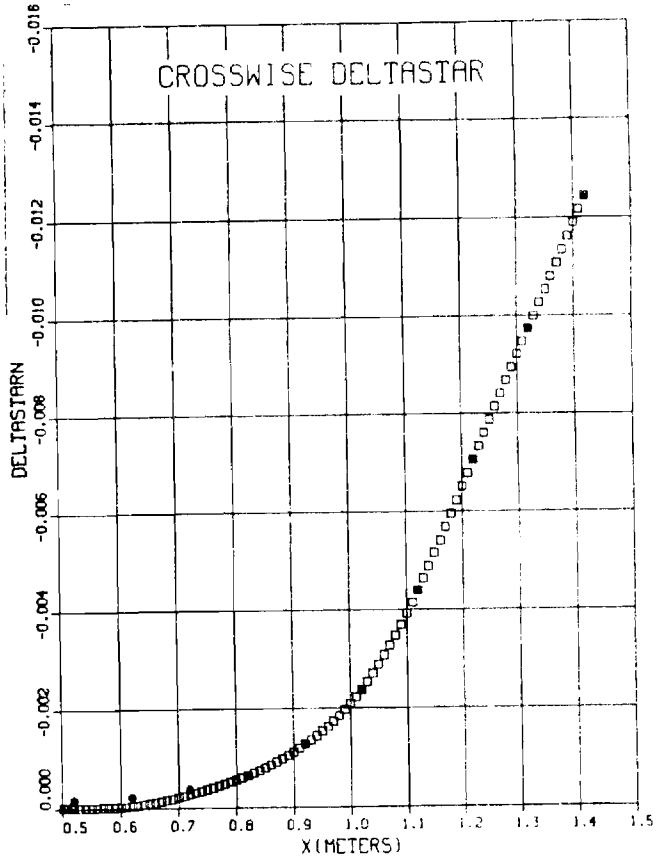

Figure 11. Displacement thickness used in the calculations with the inverse mode.

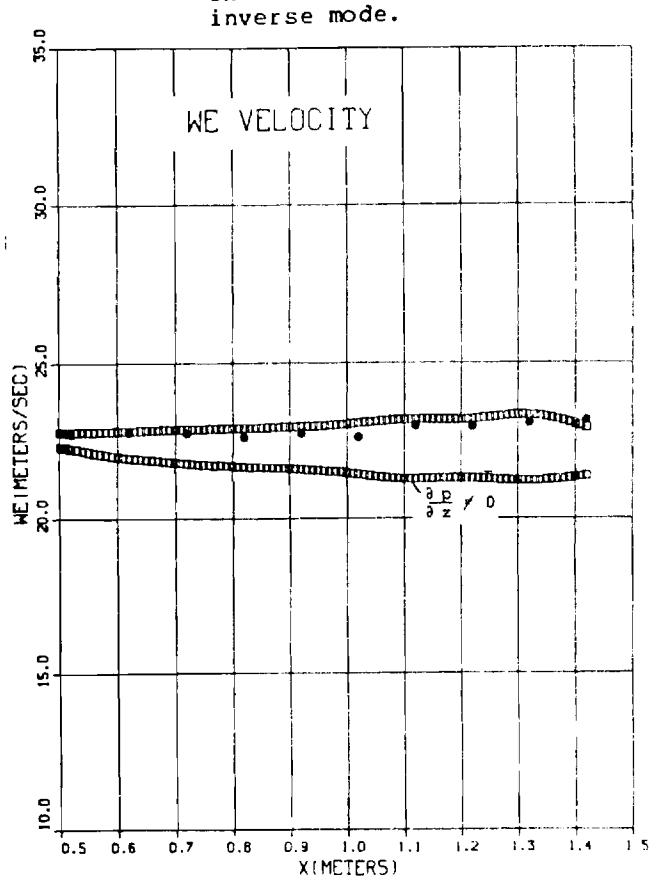

Figure 12. Calculations in the inverse mode and comparison with experiments.

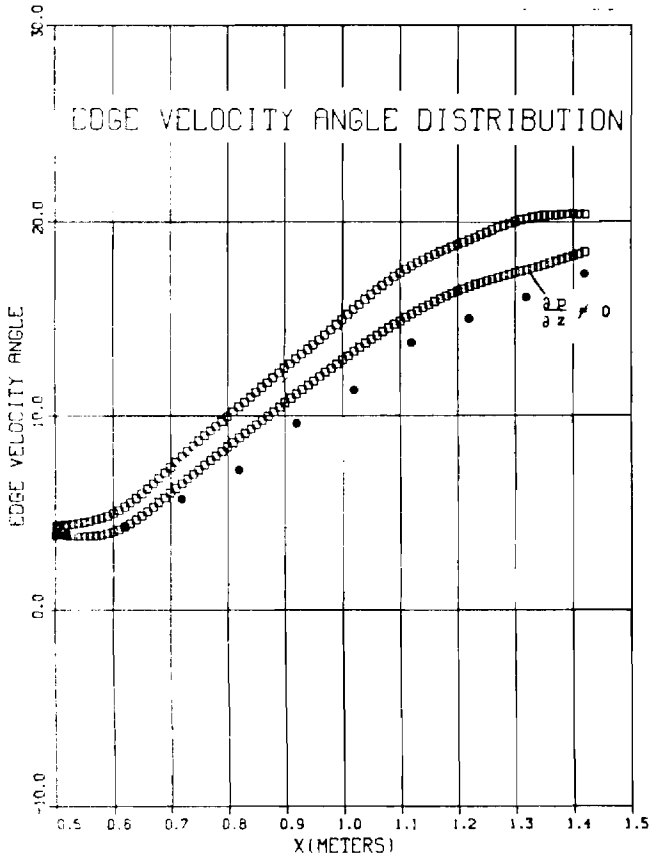

Figure 13. Calculations in the inverse mode and comparison with experiments.

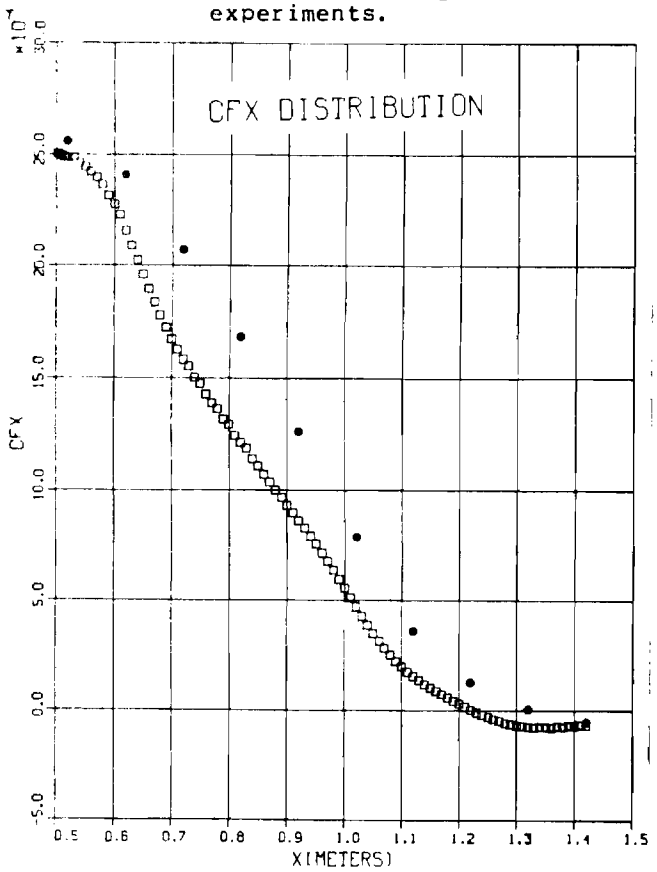

Figure 14. Calculations in the inverse mode and comparison with experiments.

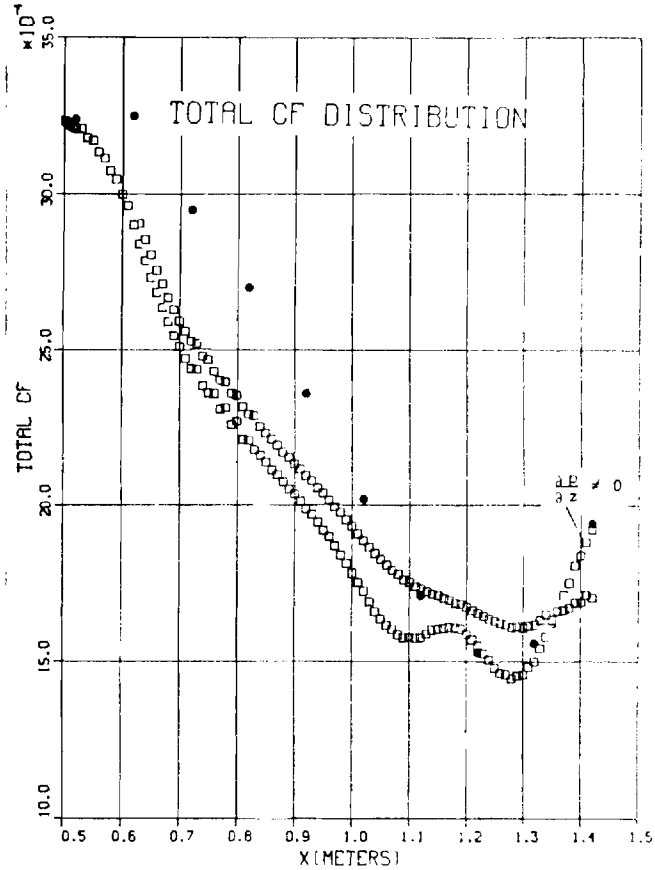

Figure 15. Calculations in the inverse mode and comparison with experiments.

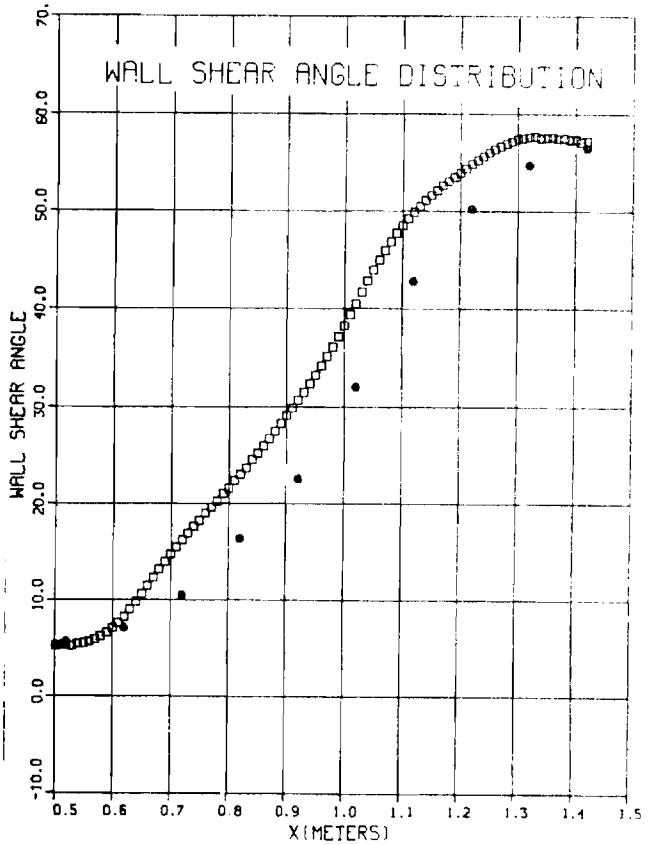

Figure 16. Calculations in the inverse mode and comparison with experiments.

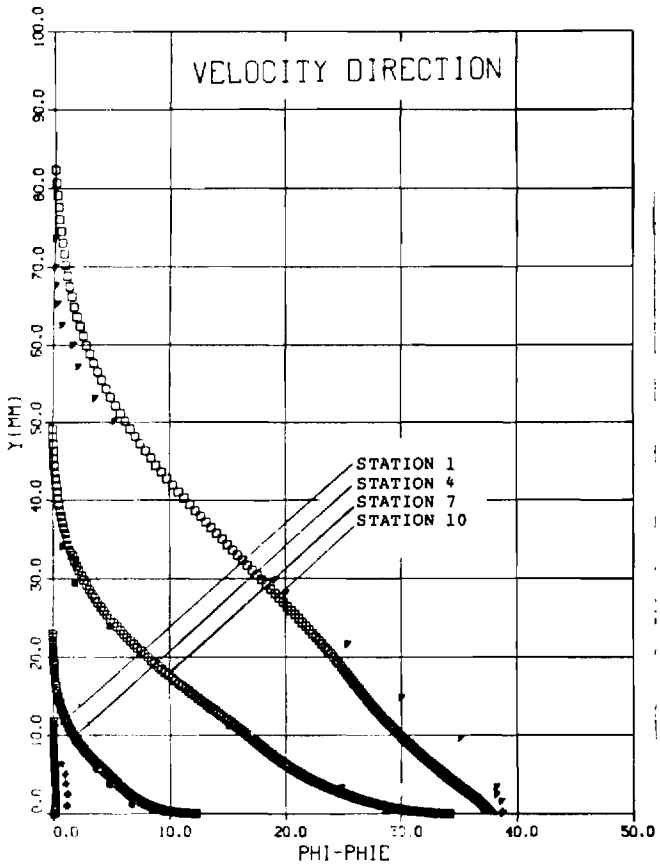

Figure 17. Calculations in the inverse mode and comparison with experiments.

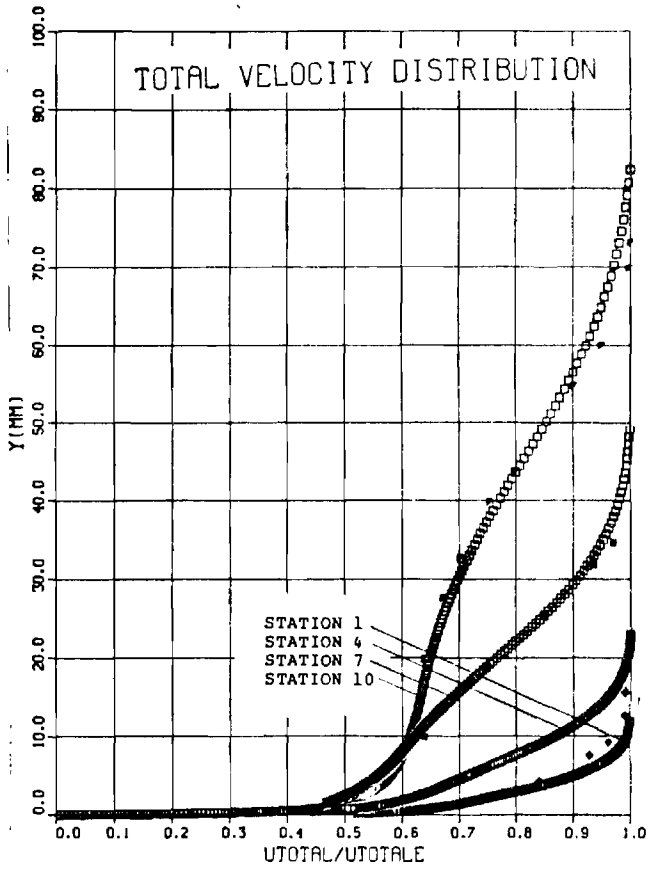

Figure 18. Calculations in the inverse mode and comparison with experiments.

Table 1

Comparison of Results from Direct and Inverse Calculations for Three-Dimensional Laminar Flow

Unit Re = 1.257×10^6, Sweep Angle = 45°)

x	$\frac{U_e}{U_{ref}}$ (Direct)	$\frac{U_e}{U_{ref}}$ (Inverse)	$c_{f_x} \times 10^3$ (Direct)	$c_{f_x} \times 10^3$ (Inverse)
0.09	0.691	0.691	1.1022	1.1020
0.11	0.688	0.688	0.9628	0.9632
0.13	0.684	0.684	0.8435	0.8425
0.15	0.680	0.680	0.7560	0.7562
0.17	0.677	0.677	0.6774	0.6765
0.19	0.673	0.673	0.6138	0.6138
0.21	0.670	0.670	0.5551	0.5545
0.23	0.666	0.666	0.5045	0.5044
0.25	0.662	0.662	0.4568	0.4564
0.27	0.659	0.659	0.4139	0.4138
x	$\frac{w_e}{U_{ref}}$ (Direct)	$\frac{w_e}{U_{ref}}$ (Inverse)	$c_{f_z} \times 10^3$ (Direct)	$c_{f_z} \times 10^3$ (Inverse)
0.09	0.707	0.707	1.1757	1.1754
0.11	0.707	0.707	1.0571	1.0570
0.13	0.707	0.707	0.9609	0.9598
0.15	0.707	0.707	0.8889	0.8885
0.17	0.707	0.707	0.8266	0.8251
0.19	0.707	0.707	0.7761	0.7754
0.21	0.707	0.707	0.7307	0.7290
0.23	0.707	0.707	0.6919	0.6909
0.25	0.707	0.707	0.6560	0.6542
0.27	0.707	0.707	0.6242	0.6229

Table 2

Comparison of Results from Direct and Inverse Calculations for Three-Dimensional Turbulent Flow

(Unit Re = 2.42×10^6, Sweep Angle = 35°)

x	$\frac{U_e}{U_{ref}}$ (Direct)	$\frac{U_e}{U_{ref}}$ (Inverse)	$c_{f_x} \times 10^3$ (Direct)	$c_{f_x} \times 10^3$ (Inverse)
0.52	0.777	0.778	2.2628	2.2743
0.62	0.769	0.765	2.2355	2.2533
0.72	0.734	0.731	1.9362	1.9504
0.82	0.691	0.688	1.6207	1.6323
0.92	0.639	0.637	1.2639	1.2758
1.02	0.599	0.597	1.0358	1.0448
1.12	0.557	0.556	0.7422	0.7562
1.22	0.536	0.536	0.7667	0.7941
1.32	0.520	0.519	0.7150	0.7462
1.42	0.504	0.504	0.6495	0.6973
x	$\frac{w_e}{U_{ref}}$ (Direct)	$\frac{w_e}{U_{ref}}$ (Inverse)	$c_{f_z} \times 10^3$ (Direct)	$c_{f_z} \times 10^3$ (Inverse)
0.52	0.629	0.624	2.0405	2.0309
0.62	0.630	0.623	2.0041	2.0040
0.72	0.632	0.620	1.9831	1.9630
0.82	0.627	0.617	1.9682	1.9361
0.92	0.630	0.613	1.9810	1.9116
1.02	0.627	0.610	1.9899	1.8999
1.12	0.636	0.606	2.0169	1.8692
1.22	0.639	0.605	2.0415	1.9095
1.32	0.644	0.604	2.0550	1.9134
1.42	0.651	0.603	2.0644	1.9178

Progress Report
on the Grant E-16-607
for the period 1/1/83 to 12/31/83

STUDIES IN THREE DIMENSIONAL TURBULENT BOUNDARY LAYER SEPARATION FROM SMOOTH SURFACES

by

S. G. Lekoudis
School of Aerospace Engineering
Georgia Institute of Technology
Atlanta, Georgia 30332
(404) 894-3014

for

The Advanced Research Organization
Department 72/11, Zone 403
Lockheed-Georgia Company
Marietta, Georgia 30063

SUMMARY

This report summarizes the work done under the Grant E-16-607 (Georgia Tech number), from the Advanced Research Organization of the Lockheed-Georgia Company, to the School of Aerospace Engineering at Georgia Tech. The viscous design problem has been addressed and solved for a certain class of three dimensional geometries. The solution is based on a combination of inverse boundary layer and inverse potential flow techniques. Progress towards an inverse boundary layer body code is made.

TABLE OF CONTENTS

1. INTRODUCTION

The main thrust of the research performed during the last calendar year has to do with the development and application of inverse boundary layer techniques. The people involved in the program are the author and Samir Radwan, a graduate student in the School of Aerospace Engineering. Mr. Radwan successfully passed his Oral Qualifying Examination for the Ph.D. degree, in February 1983. He is expected to complete the remaining requirements for his Ph.D. degree during the 1984 calendar year. These requirements are the successful completion of a thesis proposal and a successful defense of the Ph.D. thesis.

Two problems were addressed. The first is the application of inverse boundary layer calculations to the viscous design problem. The second is the development of an inverse boundary layer code for a body geometry. Progress on the first and the second problem are reported in Sections 2 and 3, and the publications and presentations that resulted from this work are in Section 4 of this report.

2. THE SWEPT WING CASE

The viscous design problem has been addressed for three dimensional flow, to the authors knowledge for the first time. This problem required the generation of geometries with prescribed aerodynamic qualities that depend on viscosity. Use have been made of inverse boundary layer and inverse potential flow methods. A swept wing was redesigned, with prescribed skin friction on part of its upper surface. Details about the method, the numerics, and the results, are in Publication 2. It is included as the Appendix of this report.

3. THE CASE OF THE ELLIPSOID

Progress towards an inverse boundary layer code for a body with a plane of symmetry is made. The numerical scheme, coded primarily by S. Radwan on Georgia Tech's CYBER-855, is briefly described next.

The three dimensional stagnation flow and the plane of symmetry flow are solved using the keller-box. The code uses marching in planes normal to the plane of symmetry, and an Alternating Direction Implicit (ADI) scheme. Therefore solutions are obtained in those planes after the planes of symmetry are computed, themselves in the inverse mode. Two-point backward derivatives are used in both the keller-box (plane of symmetry) and in the ADI (rest of surface). The target skin friction is approached iteratively by updating the pressure (see Appendix). The cross flow direction in the plane of marching is taken care by numerical differencing in the appropriate direction. The component of flow opposing the marching direction is neglected as in all inverse 3D boundary layer calculations. The ellipsoid geometry is used as a test case.

The status of the code is as follows. The three dimensional stagnation flow and the planes of symmetry have been coded and tested. The coding of the ADI in the planes normal to the direction of marching is currently being done.

4. PUBLICATIONS

The following publications are the result of the work done under the present Grant.

Non-Refereed Publications

"A Method for Designing Three Dimensional Configurations with Prescribed Skin Friction," AIAA Paper 84-0526 by S. G. Lekoudis, N. L. Sankar and S. F. Radwan, presented at the 22nd Aerospace Sciences Meeting in Reno, Nevada, on January 12, 1984.

Refereed Journal Articles

"Boundary Layer Calculations in the Inverse Mode for Incompressible Flows over Infinite Swept Wings," by S. F. Radwan and S. G. Lekoudis, to appear in the AIAA Journal.

APPENDIX

AIAA'84

AIAA-84- 0526

A Method for Designing Three-Dimensional Configurations with Prescribed Skin Friction

S.G. Lekoudis, N.L. Sankar and
S.F. Radwan, Georgia Institute of Technology,
Atlanta, GA

AIAA 22nd Aerospace Sciences Meeting

January 9-12, 1984/Reno, Nevada

A METHOD FOR DESIGNING THREE DIMENSIONAL CONFIGURATIONS WITH PRESCRIBED SKIN FRICTION

S. G. Lekoudis†, N. L. Sankar* and S. F. Radwan**
School of Aerospace Engineering
Georgia Institute of Technology
Atlanta, Georgia 30332

Abstract

This work addresses the viscous design problem for three dimensional geometries. Close to the body surface the flow is treated as a boundary layer. The design is done as follows. The skin friction distribution is the target. It is used as input in an inverse boundary layer calculation. The resulting pressure distribution is used as input for an inverse potential flow calculation and thus the surface geometry is computed. The procedure is demonstrated by redesigning a swept, tapered wing in subsonic flow. Part of the upper surface of the wing has a prescribed distribution of the skin friction.

1. Introduction

The ultimate goal of research in aerodynamics is to use the results in the design of efficient vehicles. The efficiency is related to the mission of the vehicle and the word design is reminiscent of constraints. Obtaining a shape with the desired aerodynamic qualities has always been the objective of the design engineers. Experience and trial and error have played a major part of the design process. Currently the computer helps to evaluate designs faster than in the past. However the main thrust in the use of the computer has been in the direction of inverse potential flow problems.[1] In these problems the prescribed pressure distribution serves as a boundary condition for the solution of the potential flow problem. The body geometry is computed with this solution.

The present work addresses the viscous design problem for three dimensional geometries. The target of the design is the distribution of the skin friction vector. There are several reasons for wanting to design with targets that depend on the effects of viscosity. Some of them are described in the next paragraph.

There is always demand for increased performance. Increased performance requires low drag. Large parts of the drag of airplanes and most of the drag of underwater vehicles is due to skin friction. Therefore it is desirable to have a procedure for designing three dimensional geometries with low skin friction drag. Reference 2 describes how a geometry modification can result in lesser drag in an axisymmetric body. In Reference 3, tail ends of axisymmetric bodies are designed with the objective of minimum tail length. This is achieved by keeping the boundary layer close to separation over a distance. Thus the design is done with the skin friction as target. In another application, the design of high lift airfoils requires[4,5] that the boundary layer is decelerated on the upper surface, at the maximum possible rate, without separating.

In the last two cases, the separation of the boundary layer is the limiting factor in the design. This is because of the two dimensionality of the problem. We will return to this point in Section 5 of the paper. It should be emphasized that in the above mentioned works, and in this paper, it is the pressure distribution that generates the desired skin friction. Low skin friction drag due to alteration of turbulent structures inside the boundary layer[6] is not what this paper addresses.

The method to be described is based on inverse boundary layer calculations. The input is the skin friction coefficient and the output is the pressure distribution. Solutions of the three dimensional boundary layer equations in the inverse mode have appeared recently in the literature[7-10]. The majority of the works are reported by French aerodynamicists. The solutions described in this paper are based on the method described in Reference 8. Anisotropic eddy-viscosity is used for closure. The boundary layer scheme is described in Section 2. The inverse potential formulation is in Section 3. Some remarks on the numerics are in Section 4, and the discussion of results is in the Section 5 of the paper.

2. The Inverse Boundary Layer Scheme

The equations for three dimensional boundary layers in steady, incompressible, turbulent flow over an infinite yawed cylinder, whose generator is parallel to the z-axis of an x, y, z cartesian coordinate system are:

$$\frac{\partial \overline{u^*}}{\partial x^*} + \frac{\partial \overline{v^*}}{\partial y^*} = 0 \qquad \text{(Ia)}$$

$$\overline{u^*}\frac{\partial \overline{u^*}}{\partial x^*} + \overline{v^*}\frac{\partial \overline{u^*}}{\partial y^*} = -\frac{1}{\rho^*}\frac{\partial \overline{p^*}}{\partial x^*} + \frac{\partial}{\partial y^*}\left(\nu^*\frac{\partial \overline{u^*}}{\partial y^*} - \overline{u^{*\prime}v^{*\prime}}\right) \qquad \text{(Ib)}$$

$$\overline{u^*}\frac{\partial \overline{w^*}}{\partial x^*} + \overline{v^*}\frac{\partial \overline{w^*}}{\partial y^*} = -\frac{1}{\rho^*}\frac{\partial p^*}{\partial z^*} + \frac{\partial}{\partial y^*}\left(\nu^*\frac{\partial \overline{w^*}}{\partial y^*} - \overline{w^{*\prime}v^{*\prime}}\right) \qquad \text{(Ic)}$$

In equations (I), asterisks denote dimensional quantities, bars denote time-averages, primes denote fluctuating quantities, u, v, w are the velocity components in the x, y, z direction respectively, ρ is the density, p the pressure and

† Associate Professor, Member AIAA
* Senior Research Engineer, Member AIAA
** Graduate Research Assistant, Student Member AIAA

ν the kinematic viscosity. The term $-1/\rho\,\partial p/\partial z$ is retained in order to apply the infinite yawed cylinder conditions both in an exact and in an approximate way.

We use an algebraic eddy-viscosity model for the Reynolds stresses

$$-\overline{u^{*\prime} v^{*\prime}} = \nu^* \left[(b_1 - 1) \frac{\partial \overline{u}^*}{\partial y^*} + b_2 \frac{\partial \overline{w}^*}{\partial y^*} \right] \tag{2a}$$

$$-\overline{w^{*\prime} v^{*\prime}} = \nu^* \left[(b_3 - 1) \frac{\partial \overline{w}^*}{\partial y^*} + b_2 \frac{\partial \overline{u}^*}{\partial y^*} \right] \tag{2b}$$

The anisotropic eddy-viscosity model suggested by Rotta is used to estimate the b's in Equations (2). It is described by the following relations.

$$\varepsilon_i^* = L^{*2} \left[\left(\frac{\partial \overline{u}^*}{\partial y^*} \right)^2 + \left(\frac{\partial \overline{w}^*}{\partial y^*} \right)^2 + (T-1) \frac{\left(\overline{w}^* \frac{\partial \overline{u}^*}{\partial y^*} - \overline{u}^* \frac{\partial \overline{w}^*}{\partial y^*} \right)^2}{\overline{u}^{*2} + \overline{w}^{*2}} \right] \tag{2c}$$

$$\varepsilon_o^* = 0.0168 \left| \int_o^\infty \left[(\overline{u}_e^{*2} + \overline{w}_e^{*2})^{1/2} - (\overline{u}^{*2} + \overline{w}^{*2})^{1/2} \right] dy^* \right| \tag{2d}$$

$$b_1 = \frac{\varepsilon^*}{\nu^*} (\overline{u}^{*2} + T\,\overline{w}^{*2}) / (\overline{u}^{*2} + \overline{w}^{*2}) \tag{2e}$$

$$b_2 = \frac{\varepsilon^*}{\nu^*} (1 - T)\, \overline{u}^* \overline{w}^* / (\overline{u}^{*2} + \overline{w}^{*2}) \tag{2f}$$

$$b_3 = \frac{\varepsilon^*}{\nu^*} (\overline{w}^{*2} + T\,\overline{u}^{*2}) / (\overline{u}^{*2} + \overline{w}^{*2}) \tag{2g}$$

The initial conditions for the inverse calculations can be generated in several ways. Experimental velocity profiles can be used, or velocity profiles formed by polynomial expressions, or solutions of the boundary layer equations in the direct mode can also be used. The last procedure was followed in this work. Therefore, the equations were also solved in the direct mode. The two-component vector potential used is as follows.

$$\psi^* = \sqrt{u_e^* \nu^* x^*}\, f(x, \eta) \tag{3a}$$

$$\phi^* = \sqrt{u_e^* \nu^* x^*}\, g(x, \eta) \overline{we}^* / \overline{u}_e^* \tag{3b}$$

The subscript e denotes local freestream conditions. The boundary layer coordinates are

$$x = \frac{x^*}{L^*}, \quad \eta = \frac{y^*}{x^*} \sqrt{R_x}, \quad R_x = \frac{\overline{u}_e^* x^*}{\nu^*} \quad (4, a\ b, c)$$

With the use of (3) and (4) the thin shear layer equations (1) become

$$(b_1 f'')' + \tfrac{1}{2}(1 + p_2) f'' f + p_2 (1 - f'^2) = x \left(f' \frac{\partial f'}{\partial x} - f'' \frac{\partial f}{\partial x} \right) - (b_2 g'')' \frac{\bar{w}_e}{\bar{u}_e} \tag{4a}$$

$$(b_3 g'')' + \tfrac{1}{2}(1 + p_2) f g'' + p_3 (1 - g' f') = x \left(f'' \frac{\partial g'}{\partial x} - g'' \frac{\partial f}{\partial x} \right) - (b_2 f'')' \frac{\bar{u}_e}{\bar{w}_e} \tag{4b}$$

where

$$p_2 = \frac{x^*}{\overline{u}_e^*} \frac{\overline{du}_e^*}{dx^*} \tag{5a}$$

$$p_3 = \frac{x^*}{\overline{w}_e^*} \frac{\overline{dw}_e^*}{dx^*} \tag{5b}$$

and primes denote derivatives with respect to η. The boundary conditions for the system (4) are:

$$f = f' = g = g' = 0 \qquad \text{at } \eta = 0 \tag{6}$$

$$f' = g' = 1 \qquad \text{at } \eta = \eta_e \tag{6b}$$

If c_{fx} and c_{fz} denote the local vector skin friction components in the x and z direction respectively, and c_{fx}^* and c_{fz}^* the target values, a Taylor expansion gives the following relations.

$$c_{fx}^* = c_{fx} + \frac{\partial c_{fx}}{\partial Ue} \Delta Ue + \frac{\partial c_{fx}}{\partial We} \Delta We \tag{7a}$$

$$c_{fz}^* = c_{fz} + \frac{\partial c_{fz}}{\partial Ue} \Delta Ue + \frac{\partial c_{fz}}{\partial We} \Delta We \tag{7b}$$

The relations (7) assume some proximity of the local values of the skin friction with the target values. In practice this proximity is obtained by using the velocity components of the previous location as initial guesses. From (7) one can solve for ΔUe and ΔWe and obtain

$$\Delta Ue = \frac{(c_{fx}^* - c_{fx}) \frac{\partial c_{fz}}{\partial We} - (c_{fz}^* - c_{fz}) \frac{\partial c_{fx}}{\partial We}}{\frac{\partial c_{fx}}{\partial Ue} \frac{\partial c_{fz}}{\partial We} - \frac{\partial c_{fx}}{\partial We} \frac{\partial c_{fz}}{\partial Ue}} \tag{8a}$$

$$\Delta We = \frac{(c_{fz}^* - c_{fz}) \frac{\partial c_{fx}}{Ue} - (c_{fx}^* - c_{fx}) \frac{\partial c_{fz}}{Ue}}{\frac{\partial c_{fx}}{\partial Ue} \frac{\partial c_{fz}}{\partial We} - \frac{\partial c_{fx}}{\partial We} \frac{\partial c_{fz}}{\partial Ue}} \tag{8b}$$

The expressions (8) are used to obtain the increments in the components of the freestream velocity, during the iteration procedure. This way of computing the inverse amounts to solving the direct problem iteratively until the desired boundary condition is achieved. We decided against using the skin friction directly as a boundary condition. That would have resulted in solving the boundary layer equations with all conditions at the wall.

3. The Inverse Potential Flow Scheme

The inverse potential flow method used is similar to the procedure described in Reference 11. The procedure can be used to design wing alone configurations at subsonic and transonic speeds. Several applications of the procedure are given in Reference 1. We will briefly describe some details of the procedure.

At each span station, the wing profile (x, y) is unwrapped about a singular point (x_o, y_o), located just inside the trailing edge. The resulting smoothly varying curve (A_o, S_o) is described by the following relations:

$$x = x_o + A_o^2 - S_o^2 \tag{9}$$

$$y = y_o + 2A_o S_o \tag{10}$$

Additional stretching and shearing transformations are then used to map the physical domain (x, y, z) onto a computational domain (ξ, η, ζ).

The design proceeds as follows. For a given wing shape, several relaxation sweeps produce a current value for the surface velocity q. If the target velocity is denoted by Q, the following equation is solved in pseudo-time:

$$\beta_o \frac{\partial S}{\partial t} - \beta_1 \frac{\partial^3 S}{\partial \xi^2 \partial t} + \beta_2 \frac{\partial^2 S}{\partial \xi \partial t} = Q^2 - q^2 \tag{11}$$

Clearly as Q approaches q, $\frac{\partial S}{\partial t} = 0$ and no further changes in the wing shape are performed. The Equation (11) is discretized at any (i,j) point on the wing surface as follows:

$$\beta_o \frac{\partial S}{\partial t} \cong \beta_o (S_{oij}^{new} - S_{oij}^{old})/\Delta t = \beta_o \frac{\Delta S_{oij}}{\Delta t} \tag{12}$$

$$\beta_1 \frac{\partial^3 S}{\partial \xi^2 \partial t} \cong \beta_1 (\Delta S_{oi+i,j} - 2\Delta S_{oij} + \Delta S_{oi-l,j})/(\Delta \xi^2 \Delta t) \tag{13}$$

On the upper surface where the flow direction is from i to i+l,

$$\beta_2 \frac{\partial^2 S}{\partial \xi \partial t} \cong \beta_2 (\Delta S_{oi+l,j} - \Delta S_{oi,j})/(\Delta \xi \Delta t) \tag{14}$$

While on the lower surface where the flow direction is from i to i-l,

$$\beta_2 \frac{\partial^2 S}{\partial \xi \partial t} \cong \beta_2 (\Delta S_{oi-l,j} - \Delta S_{oij})/(\Delta \xi \Delta t) \tag{15}$$

The sign of β_2 on the upper and lower surfaces is chosen so that the coefficient of the ΔS_{ij} term in the resulting tridiagonal equation is augmented. At each span station (j = constant) the discretization leads to a system of tridiagonal equations for ΔS_{ij}. Closed trailing edges can be obtained by setting $\Delta S_{ij} = 0$ at the two points in the upper and lower surface at the trailing edge. The tridiagonal system is solved using the Thomas algorithm. The coefficients β_o, β_1, β_2 are user supplied constants, chosen for rapid and stable convergence of the potential flow sweeps and of the wing surface design calculations.

4. The Numerical Procedure

The system of equations (4) is solved using the Keller box[12], by transforming it into a system of first order equations. The following dependent variables are used

$$f = F_1 \qquad g = F_2 \tag{16a}$$

$$f' = U_1 \qquad g' = U_2 \tag{16b}$$

$$f'' = V_1 \qquad g'' = V_2 \tag{16c}$$

The system of Equations (4) can then be written in the form

$$F_1' = U_1 \tag{17a}$$

$$U_1' = V_1 \tag{17b}$$

$$(b_1 V_1)' = -\frac{1}{2}(1 + P_2)V_1 F_1 - P_2(1 - U_1^2) + x\left(U_1 \frac{\partial U_1}{\partial x} - V_1 \frac{\partial F_1}{\partial x}\right)$$

$$- (b_2 V_2)' \bar{We}/\bar{Ue} \tag{17c}$$

$$F_2' = U_2 \tag{17d}$$

$$U_2' = V_2 \tag{17e}$$

$$(b_3 V_2)' = -\frac{1}{2}(1 + P_2)F_1 V_2 - P_3(1 - U_1 U_2) + x\left(V_1 \frac{\partial U_2}{\partial x} - V_2 \frac{\partial F_1}{\partial x}\right) - (b_2 V_1)' \bar{u}e/\bar{w}e \tag{17f}$$

The Equations (17a, b, c) and (17d, e, f) are solved using the standard box. A Newton iteration and a block-tridiagonal inversion (3 x 3) is used. The Equations (17d, e, f) were not linearized, but solved after the solution of the Equations (17a, b, c) provided, at each iteration, the values of F_1, U_1, V_1. Convergence was achieved by allowing the calculation to stop when the percentage change of V_1 and V_2 was less than a prescribed tolerance. This tolerance was achieved for the twenty, closest to the wall, points in the boundary layer.

The partial derivatives of c_{fx} and c_{fz} in Equation (8) were evaluated using increments δUe and δWe with δ controlled from input. Convergence was judged by the percentage changes in both velocities (Ue, We) and skin friction coefficients (c_{fx}, c_{fz}). The boundary layer equations were then solved in the direct mode, three times per iteration, and the $\partial c_{fx}/\partial Ue$, $\partial c_{fx}/\partial We$, $\partial c_{fz}/\partial Ue$, $\partial c_{fz}/\partial We$, were computed using a first order finite-difference approximation. For example, if Ueo and Weo were the current values of the freestream velocity components, and c_{fx1} and c_{fz1} the current values of the skin friction, a new calculation was performed with $Ueo(1 + \delta)$ and Weo as the freestream velocity components. This resulted in new c_{fx2} and c_{fz2}. Then

$$\frac{\partial c_{fx}}{\partial Ue} = \frac{c_{fx2} - c_{fx1}}{\delta Ueo} \tag{18a}$$

$$\frac{\partial c_{fz}}{\partial Ue} = \frac{c_{fz2} - c_{fz1}}{\delta Ueo} \tag{18b}$$

The same procedure was used for the $\partial/\partial We$ derivatives and then the velocities were updated by using (8) and (9) as follows

$$U_e = Ueo + \Delta Ue \qquad (19a)$$

$$We = Ueo + \Delta We \qquad (19b)$$

In Reference 8, where the input displacement thickness was translated into a boundary condition for the inverse calculations, upwinding was found necessary in order to obtain smooth solutions. In this work where the input skin friction was approached iteratively, there was no need for upwinding. This may be due to the fact that the input boundary condition was achieved only within a prescribed tolerance.

5. Discussion of Results

In order to check the inverse calculations, the following exercise was carried out. We run the boundary layer code with a prescribed pressure distribution, in the direct mode. The computed skin friction was kept in a file, with four significant digits retained. It was then used as input for a run in the inverse mode. Figures 1 and 2 show the comparison between the components of the freestream velocity, used as input, and the ones computed from the inverse code. The agreement is good. It could be mentioned that in the direct mode, the pressure gradients are computed using backward differences.

A particular wing was selected as the basic configuration. The wing has a sweep of 25 degrees at the quarter chord, aspect ratio 8 and taper ratio 0.4. It is described in detail as wing A in Reference 13. The calculations are for a unit Reynolds number of 10^6 and the streamwise length of the wing root is 5.78 units of length. The freestream Mach number used, 0.15, makes the error due to the incompressible flow assumptions in the boundary layer very small.

For reasons of simplicity, and because the procedure does not include wake calculations, the target skin friction was described only on part of the upper surface of the wing. The leading and trailing edge regions are excluded. The boundary layer is solved on all of the 22 span stations, and the solution points on the surface coincide with the locations that the solution is provided from the potential flow code. The local sweep is used, and for a wing with the characteristics mentioned before, the infinite swept wing assumptions[8] are reasonable to make. The surface coordinate S is measured from the leading edge line, and on the airfoil normal to the leading edge. Since the leading and trailing edge regions are excluded, the curvature terms are not included in the boundary layer calculations through the metrics. The length c is the local chord length of the airfoil normal to the leading edge.

The boundary layer is tripped at a fixed point after the leading edge, at approximately the location of the peak suction close to $S/c \cong .05$. In the inverse mode, the calculations start at a fixed streamwise point, close to $S/c \cong .16$. The direct mode is used up to that point. The isotropic eddy-viscosity, $T = 1.0$, is used in all the cases.

The design is done as follows. Excluding a region around the midchord of the upper surface, the skin friction values, and therefore the pressure, are kept unchanged, and equal to the values computed from the direct mode on the wing. Figures 3 and 4 show the imposed linear variation of c_{fx} and c_{fz}. It raises the c_{fz} and lowers the c_{fx} values, in the region approximately $.16 < S/c < .74$, on the upper surface. As expected, the computed components Ue and We of the local freestream velocity follow the trend of the skin friction values, and they are shown in Figures 5 and 6. This imposed rotation of the skin friction vector in the outboard, spanwise, direction may be accomplished without excessive thickening of the boundary layer. This turning of the skin friction vector reduces its drag producing component. It is not possible to be done in two dimensional or axisymmetric bodies because of the flow geometry. However excessive turning may cause boundary layer separation.

Separation of a three dimensional boundary layer cannot, as in two dimensions, be characterized by the vanishing of the skin friction. Although the direction of the skin friction vector can be taken as an indication of separation, it is much safer to refer to separation in three dimensions when the shear layer lifts off from the body and goes into the potential flow. The occurrence of this event, which will generate pressure drag, has to be avoided. Therefore a design of a body with low skin friction in three dimensions depends on accurate predictions of the interplay between the turning of the skin friction vector and the occurrence of separation. It should be remembered that, for the case of lifting surfaces, the requirements on the pressure distributions may preclude certain ranges of this turning.

The pressure distributions in Figures 7, 8 and 9 show the effect of the imposed skin friction. Because no effort was made to prescribe a target skin friction, so that the new and the original pressures are joined smoothly, the following is observed. A discontinuity in the pressure distribution is generated at approximately $S/c \cong 0.74$. The inverse potential code smoothed it somewhat and, as it should, produced airfoils with an abrupt change of profile slope at that location.

The redesigned wing sections at the 25, 50 and 75 percent span locations are shown in Figures 10, 11 and 12. There is a flattening of the upper surface, similar to the one observed in high lift airfoils[3]. As mentioned the sudden acceleration at $S/c \cong 0.74$ produced a discontinuity of the profile slope at that location. It was not possible to impose the target skin friction, shown in Figures 3 and 4, on the whole upper surface of the wing. When this was done, the design pressures failed to match the target pressures close to the wing tip. Therefore, starting at span station 17, and up to the last (22nd) station at the wing tip, the design skin friction was the linear interpolation between the values at station 17 and the original values at the tip. This procedure generated design pressures close to the target for the whole wing.

The results presented are a very small sample of the possible choices. However they demonstrate a viable procedure for solving the viscous design problem in three dimensional flow. Designs with strong viscous/inviscid interaction effects have to be attempted by using the present method after the two inverse codes are coupled.

6. Concluding Remarks

A method has been developed for designing three dimensional geometries with prescribed skin friction. It has been demonstrated by redesigning a swept wing in subsonic flow. The following remarks seem appropriate.

1. The work extends ideas already applied in two dimensional problems to the three dimensional case.

2. It can be used to design with specification of the skin friction as the target. Therefore it can be used for designing for low drag, high lift, or avoidance of separation.

3. It could be extended to compressible flow, where it could be used to locate shocks through sudden skin friction rise.

4. The questions of uniqueness of the solutions, already complicated in the transonic (potential) flow case, should be carefully investigated.

Acknowledgement

The first and last authors were supported by a Grant from the Advanced Research Organization of the Lockheed-Georgia Company.

References

1. Burris, C.B., Heney, P.H. and Sankar, N.L., "Computational Aerodynamic Design of Advanced Transport Aircraft," AIAA Paper 83-1865.

2. Lin, J.C., Walsh, M.J., Watson, R.D. and Balasubramaniam, R., "Turbulent Drag Characteristics of Small Amplitude Rigid Surface Waves," AIAA Paper 83-0228.

3. Smith, A.M.O., Stokes, T.R. and Lee, R.S. "Optimum Tail Shapes for Bodies of Revolution," J. Hydronautics, Vol. 15, No. 1-4, pp. 67-73, 1981.

4. Liebeck, R.H., "Design of Subsonic Airfoils for High Lift," Vol. 15, No. 9, pp. 547-561, 1978.

5. Lissaman, P.B.X., "Low Reynolds Number Airfoils," Annual Review of Fluid Mechanics, 1983.

6. Hefner, J.N., Anders, J.B. and Bushnell, D.M., "Alteration of Outer Flow Structures for Turbulent Drag Reduction," AIAA Paper 83-0293.

7. Cousteix, J. and Houdeville, R., "Singularities in Three Dimensional Turbulent Boundary Layer Calculations and Separation Phenomena," AIAA Journal, Vol. 19, No. 8, pp. 976-985, 1981.

8. Radwan, S.F. and Lekoudis, S.G., "Boundary Layer Calculations in the Inverse Mode for Incompressible Flows Over Infinite Swept Wings," AIAA Paper 83-0228 (to appear in AIAA Journal).

9. Delery, J.M. and Formery, M.J., "A Finite Difference Method for Inverse Solutions of 3-D Turbulent Boundary Layer Flow," AIAA Paper 83-0301.

10. Wington, L.B. and Yoshihara, H., "Viscous-Inviscid Interactions with a Three Dimensional Inverse Boundary Layer Code," Second Symposium on Numerical and Physical Aspects of Aerodynamic Flows, California State University, Long Beach, January 17-20, 1983.

11. Bauer, B., Garabedian, P. and McFadden, G., "The NYU Inverse Swept Wing Code," NASA CR-3662, January 1983.

12. Bradshaw, P., Cebeci, T. and Whitelaw, J., Engineering Calculation Methods for Turbulent Flow, Academic Press, 1981.

13. Hinson, B. L. and Burdges, K.P., "An Evaluation of Three-Dimensional Transonic Codes Using New Correlation-Tailored Test Data," AIAA Paper 80-0003.

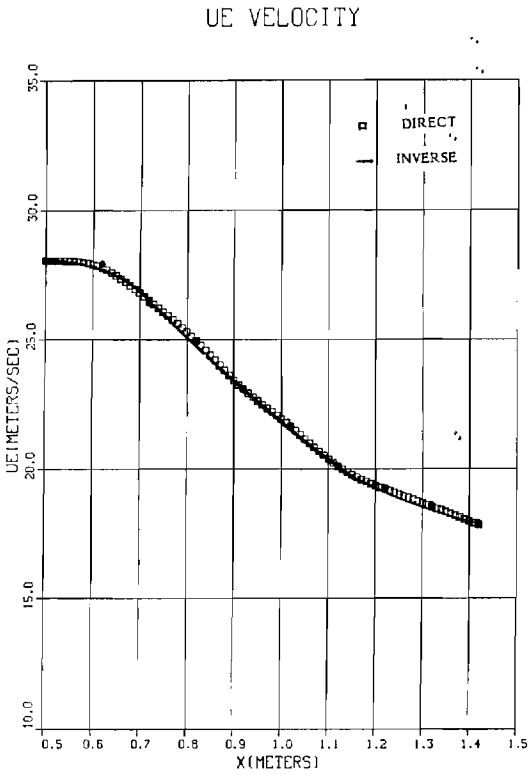

Figure 1. Comparison of input (direct) and predicted (inverse) edge velocity component

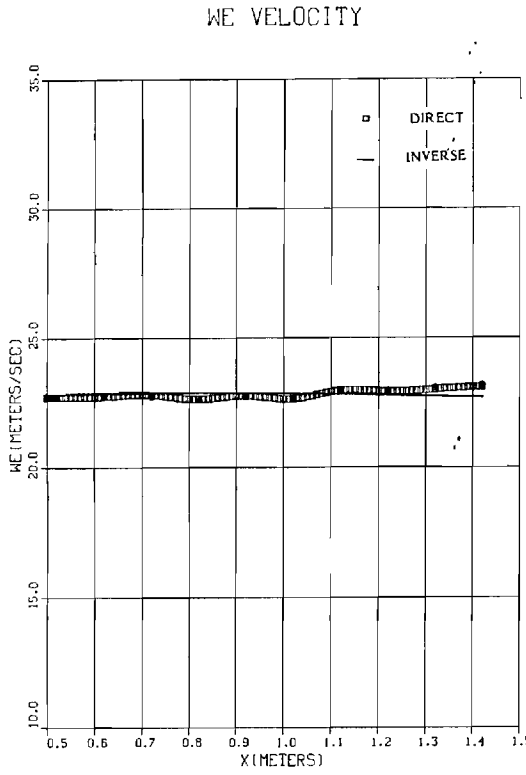

Figure 2. Comparison of input (direct) and predicted (inverse) edge velocity component

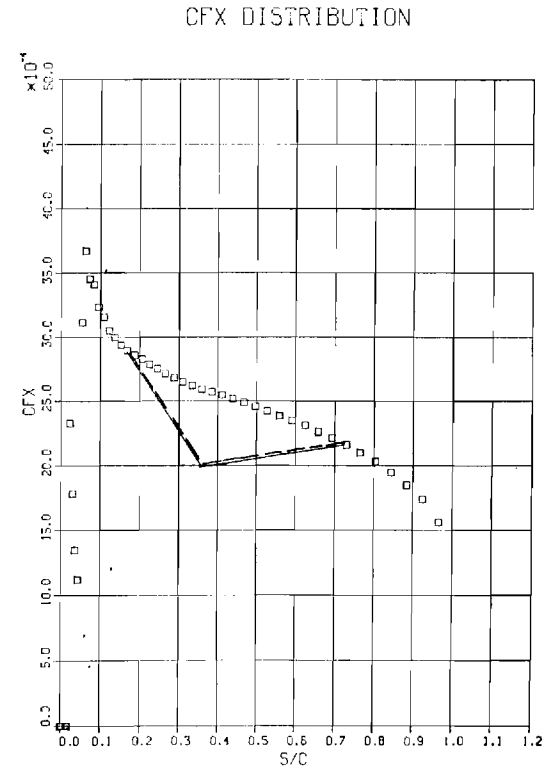

Figure 3. Original (□) and target (—,---) skin friction component at 25% span

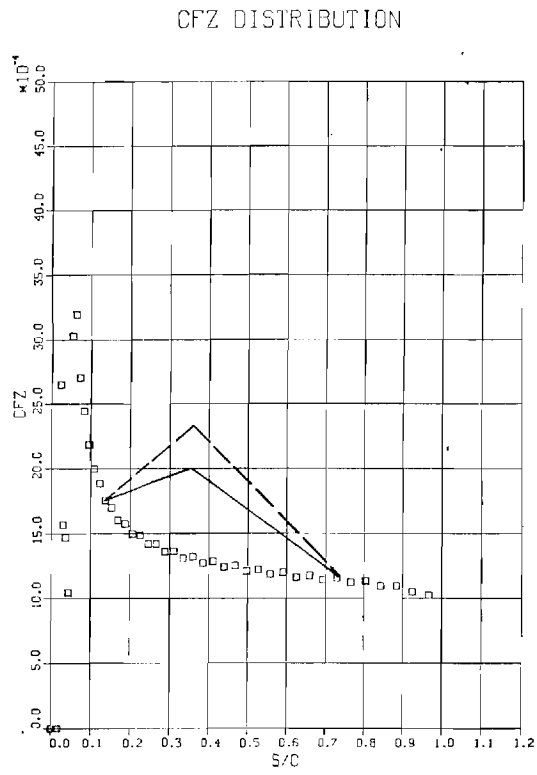

Figure 4. Original (□) and target (—,---) skin friction component at 25% span

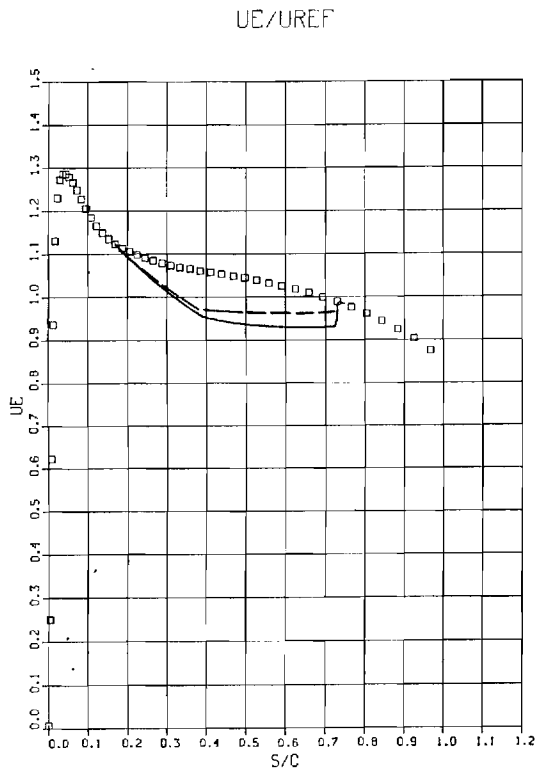

Figure 5. Original (□) and new (—,---) edge velocity component at 25% span

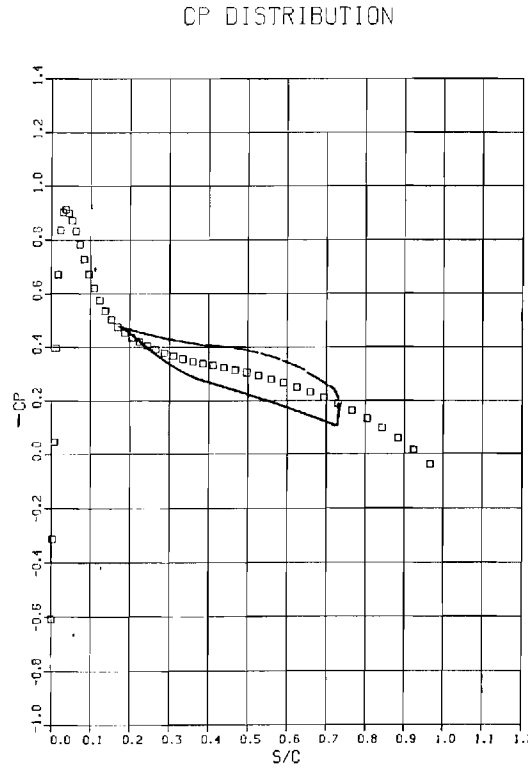

Figure 7. Original (□) and new (—,---) pressure distribution at 25% span

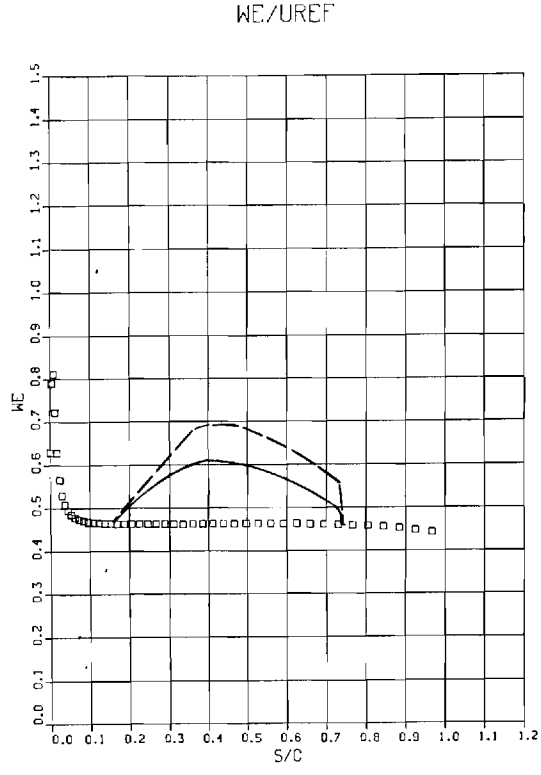

Figure 6. Original (□) and new (—,---) edge velocity component at 25% span

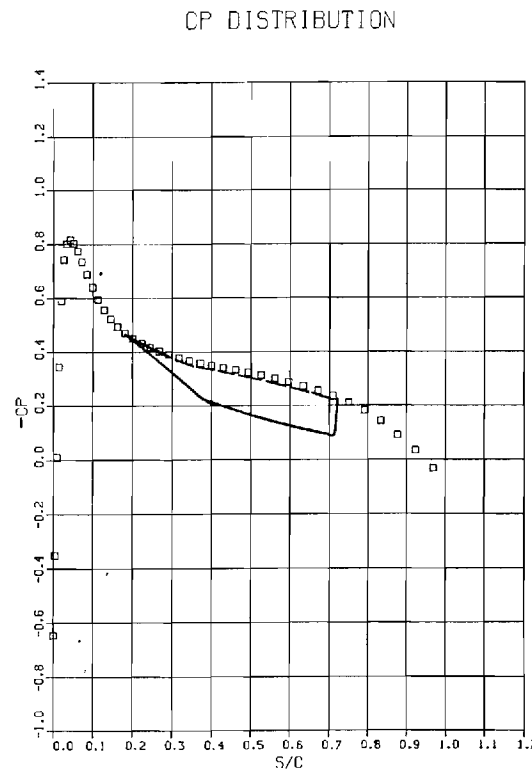

Figure 8. Original (□) and new (—,---) pressure distribution at 50% span

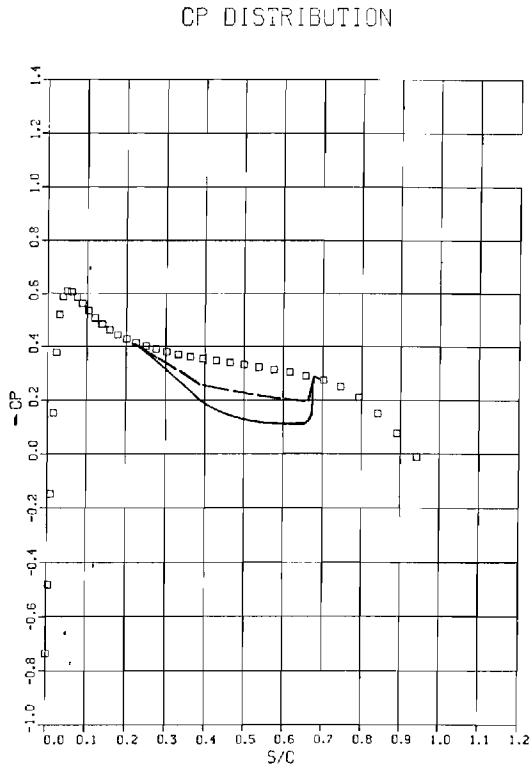

Figure 9. Original (□) and new (—,--) pressure distribution at 75% span

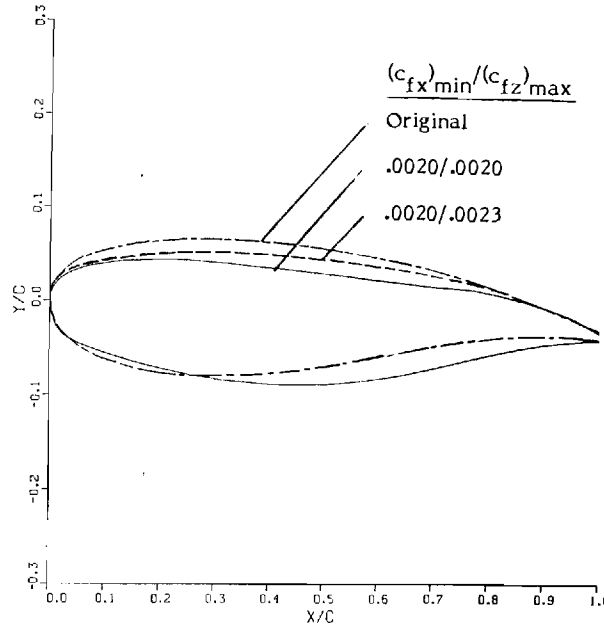

Figure 11. Streamwise airfoil shapes at 50% span

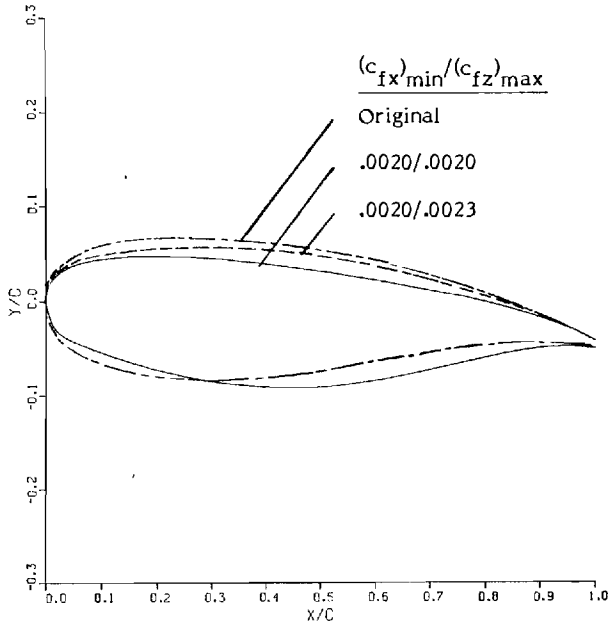

Figure 10. Streamwise airfoil shapes at 25% span

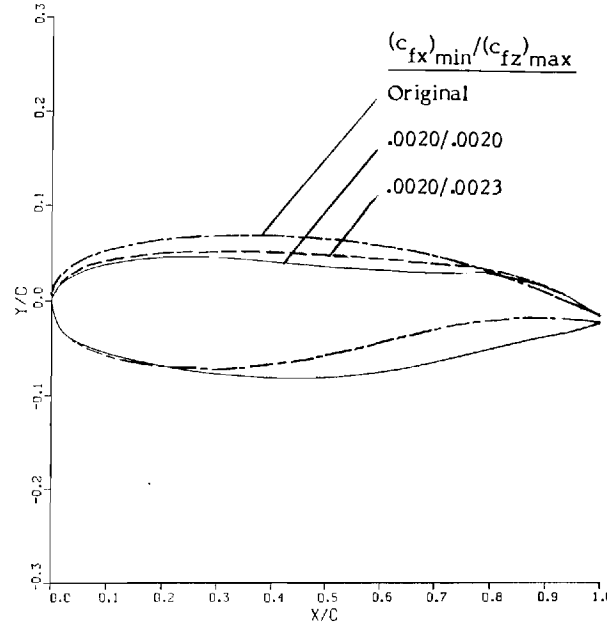

Figure 12. Streamwise airfoil shapes at 75% span